Refining the high-fidelity archaeointensity curve for western Europe over the past millennium: analysis of Tuscan architectural bricks (Italy)

Agnes Genevey, Claudia Principe, Yves Gallet, Giuseppe Clemente, Maxime Le Goff, Alexandre Fournier, Pasquino Pallecchi

Refining the high-fidelity archaeointensity curve for Western Europe over the past millennium: Analysis of Tuscan architectural bricks (Italy)

Agnès Genevey, Sorbonne Université, CNRS, Laboratoire d'Archéologie Moléculaire et Structurale, LAMS, 4 place Jussieu, F-75005 Paris, France.

Claudia Principe, Istituto di Geoscienze e Georisorse, Area della Ricerca CNR, Via G. Moruzzi 1, 56124 Pisa, Italy & IGG-CNR Archaeomagnetic Dating Laboratory (ARCHAEO-Lab), Villa Borbone, Viareggio, Italy

Yves Gallet, Université de Paris, Institut de Physique du Globe de Paris, CNRS, 1 rue Jussieu, F-75005 Paris, France

Giuseppe Clemente, Independent researcher, via vittorio Galluzzi 8, I-56124 Pisa, Italy

Maxime Le Goff, Université de Paris, Institut de Physique du Globe de Paris, CNRS, 1 rue Jussieu, F-75005 Paris, France

Alexandre Fournier, Université de Paris, Institut de Physique du Globe de Paris, CNRS, 1 rue Jussieu, F-75005 Paris, France

Pasquino Pallecchi, Laboratori di Restauro e Diagnostica, Soprintendenza Archeologia, Belle Arti e Paesaggio per la Città Metropolitana di Firenze e le Province di Pistoia, Prato e Firenze, Italy

Keywords: Archaeomagnetism, Archaeointensity, Palaeomagnetic secular variation, Italy, Western Europe, Past Millennium

Abstract

New archaeointensity results were obtained from fourteen groups of baked-brick fragments collected in and around Pisa (Tuscany, Italy). The fragments were assembled from civil and

religious buildings whose dating of construction or renovation, over the past millennium, was constrained by documentary sources. This collection, analysed using the Triaxe protocol, was found particularly suitable for intensity experiments, with a success rate of ~84% corresponding to 276 fruitful specimens associated to 125 independent brick fragments. The Tuscan data clearly show a peak in intensity at the transition between the 16th and 17th centuries. They also are in very good agreement and are complementary to a dense dataset previously obtained in France. Considering the results available within a 700 km radius of Beaune (between Paris and Pisa), all satisfying a set of quality criteria, a mean geomagnetic field intensity variation curve was constructed for the past millennium using a newly developed transdimensional Bayesian technique. This curve, which thus incorporates the new Tuscan results, allows a better recognition of three intensity peaks (during the twelfth, the fourteenth, and around AD 1600) in Western Europe. The detail of this curve is a clear illustration of the centennial-scale resolution that can be achieved using accurate archaeointensity data.

1. Introduction

Due to its active volcanoes and particularly rich cultural heritage, Italy can certainly be viewed as a privileged "playground" for palaeomagnetists to trace back recent variations of the Earth's magnetic field. Analysis of lava and pyroclastic flows emitted by Italian volcanoes has enabled important steps in understanding and describing the main lines of the geomagnetic directional variations over the past few millennia (e.g. Tanguy et al., 1999, 2003, 2007, 2012; Principe et al. 2004; Arrighi et al. 2006; Vezzoli et al. 2009; Branca et al. 2015a). Additionally, these studies further allowed re-dating of some lava flows – in the case of Mount Etna and Vesuvius, these archaeomagnetic constraints were ultimately incorporated

for drawing their respective most recent geological map, underlining the potential of such studies for the comprehension of volcanic edifices (Branca et al. 2015b; Paolillo et al., 2016)

On the other hand, during the past 15 years or so, there has been in Italy a dynamic development of archaeomagnetic research *sensu stricto*. New archaeodirectional data were acquired from in situ fired structures, which, together with volcanic data, have allowed a continuous and accurate description of the main lines of the geomagnetic directional variations in the Italian Peninsula from 1200 BC onwards (see the compilation of Tema et al. 2006 updated in 2011 by Tema, and new results acquired since then: Malfatti et al. 2011; Kapper et al. 2014; Tema et al. 2016).

In contrast, archaeointensity data in Italy remains very few, despite recent progress. Only 31 results are currently available for a large time interval of eight millennia, with a quite uneven temporal distribution (Evans 1986, 1981; Aitken et al. 1988; Hedley and Wagner 1991; Hill et al. 2007, 2008; Donadini and Pesonen 2007; Gallet et al. 2009; Tema et al. 2010, 2013, 2016 see also Tema et al. 2011). A few other archaeointensity results were obtained in Italy, but they mostly relied on archaeomagnetic dating, and for this reason they were not further considered in this study (e.g. Tema et al. 2015; Principe et al. 2018). Most of the available results (21) are dated between the 3rd century BC and the 8th century AD, with a strong concentration of data (12) between 100 BC and AD 100. Three archaeointensity results were recently obtained for the Early Neolithic period (c. 7500 years ago; Tema et al. 2016), two results are dated for the 8th century BC and the five remaining results of 31document the past five centuries. New archaeointensity data are thus required before a full description of the geomagnetic field variations in Italy over the past two to three millennia can be achieved.

This study aims to contribute to this long-term project with the archaeointensity analysis of groups of brick fragments collected in and around Pisa. Fourteen brick buildings dated from between the middle of the 12th century and the end of the 17th century were

75 sampled. From a broader geomagnetic perspective, this study also addresses the issue of the
76 maximum time resolution of the recording of the geomagnetic field intensity variations
77 accessible from archaeomagnetic data. This is particularly important as several short-term
78 (maximum of two centuries) intensity peaks have been proposed over the past millennium in
79 Western Europe from a dense set of French data (Genevey et al. 2009, 2013, 2016). The
80 intensity variation rates associated with these peaks are quite strong (~0.10 μT/yr), similar to
81 the maximum rate observed in the recent field (e.g. Livermore et al., 2014).
82
83 **2. Description of the historical baked-brick buildings investigated**
84 Since the Middle Ages, Pisa and its province have been an important area in Tuscany
85 for ceramic production, particularly using clay from the Arno River and the Serchio River
86 (Clemente 2015, 2017). Bricks are still produced in Pisa, and numerous buildings made of
87 bricks were built during the past eight centuries of Pisa's history.
88 Our sampling focused on the baked-brick architectural heritage of the city of Pisa and
89 its neighbouring territory, encompassing almost five and a half centuries, from the middle of
90 the 12th century to the end of the 17th century. It thus explores the history of Pisa from its
91 apogee as a maritime and commercial power to its decline at the end of the 13th century,
92 followed by a lengthy period under the domination of Florence.
93 We selected a series of fourteen ensembles of bricks based on careful analysis of
94 available historical and archaeological data, incorporating documentary, iconographic and
95 cartographic sources. In one case, the year of inauguration was directly inscribed on the
96 building (Figure 1a,b). All bricks were collected from important buildings commissioned by
97 the political and/or religious authorities. Even though the year of construction/inauguration of
98 such buildings do not necessarily correspond exactly to the year of production of the bricks, it
99 is nevertheless certain that the time lag between their production and their use was very short

100 (most probably less than a year). According to historical and archaeological evidence, the
101 bricks used were produced specifically for each construction and were not recycled, also
102 because the quantities of bricks required were extremely high. Furthermore, in order to avoid
103 the sampling of possibly re-used bricks, we have taken great care to take all our samples from
104 parts of the walls characterized by homogeneous bricks in terms of colour, aspect, and
105 dimension. No damaged brick, particularly with traces of burning or chipped portions, were
106 sampled. In addition, to ensure that the sampled bricks had a size characteristic of the
107 expected period, we used mensiochronology, a chronological tool based on the temporal
108 evolution of brick size (e.g. Quiros Castillo 1997). Although this tool requires improvement,
109 it was observed that the thickness of the bricks gradually decreased from ~6 cm around 1200
110 to ~4 cm at ~1700 (Quiros Castillo 1997). Furthermore, our selection of sites was dictated by
111 their accessibility to our sampling (Table 1). This sampling was performed using a portable
112 driller. Between 10 and 16 cores were taken per group, and the holes were later filled with
113 tinted mortar in order to restore the visual aspect of the sampled walls as much as possible
114 (Figure 1c,d,e).
115 Nine groups were collected in Pisa. The two oldest (Pise11 and Pise12) are from the medieval
116 ramparts built between the middle of the 12th century and the 14th century. These are largely
117 preserved and still partly surround the historical centre of the city. Drilling was performed on
118 the same wall located on the edge of the present Scotto Garden (south bank of the Arno
119 River), where two different phases of construction of the rampart are observed (Gattiglia and
120 Milanese, 2006). The construction of this medieval wall was initiated in AD 1155 and the
121 bricks of group Pise12 document this first phase, as confirmed by their thickness, between 6.5
122 and 7.5 cm, larger than the one observed since. The second, more recent, sampled phase
123 (Pise11) dates from the first half of the 14th century – i.e., the end of the construction of the
124 city wall (Quiros Castillo 1997).

Two groups were sampled in the Florentine fortress located in the same area of the Scotto Garden. This large building was erected during the middle of the 15th century (AD 1440), after the end of the Pisan Republic and under Florentine domination (Gattiglia and Milanese 2006). The first group of samples (Pise10) collected in the Santa Barbara tower (northern part of the fortress) dates from its construction, whereas the second group from the Sangallo bastion (Pise09; north-western part near the Florentine bridge over the Arno River, inside the Corsini building) corresponds to a renovation phase, during AD 1531–1533, which occurred after a short period of revolt in Pisa and its subsequent reconquest by Florence. Another group (Pise02) was collected from the Oratory of San Bernardino, which was built at the end of the 15th century to ward off epidemics of medieval plague (Sodi and Radi 1979).

In addition to group Pise09, three other archaeomagnetic groups allow us to document the 16th century. Group Pise01 was collected from the hydraulic regimentation structure of the 'Bocchette', positioned at the entrance of a canal built during the years of Cosimo I de' Medici's government and located a little to the east of the city (Figure 1a,b). This structure was constructed to divert excess waters of the Arno River towards the Pisan plain, thus avoiding devastating flooding inside the city (Ciuti 2003). Group Pise08 was sampled in the important structure of the Medici arsenal, built between 1543 and 1563 on the banks of the Arno River towards its mouth (Ciuti 2003). Our sampling concerns a well-known renovation phase carried out few years later in 1588. The third group (Pise06) was sampled in the structure of the Medici aqueduct, the construction of which was decided upon by Grand Duke Ferdinando I de' Medici. This aqueduct provided Pisa with fresh and drinkable water from the source, located near the little town of Asciano in the Monti Pisani area (Gasperini et al. 2015). This archaeomagnetic fragment group was collected in a pillar of the terminal segment of the structure.

In Pisa, the 17th century is represented by a group of fragments collected from the Santo Stefano Dei Cavaleiri church located in the city centre. Although it was founded around the middle of the 16th century under the direction of Cosimo I de' Medici, some parts of its external walls are more recent and precisely date to 1683–1691 (Sodi and Renzoni 2003), where archaeomagnetic group Pise07 comes from.

Five more groups of fragments were collected in the province of Pisa. The first group (Tosc03) dates from the second half of the 13th century and was sampled in a tower of the castle of Calcinaia, a small medieval city of the Pisan plain along the Arno River (17 km from Pisa), that was built and fortified by the Pisans (Alberti and Baldassarri 2004). A second group (Tosc04) was precisely dated to 1331, as ascertained by archives, and was drilled in the external wall of the church of Marti in the municipality of Montopoli Valdarno (Febbraro 2006). Finally, three archaeomagnetic fragment groups were also sampled in other segments of the Medici aqueduct dated to slightly more recent ages (first half of the 17th century) than group Pise06 located in Pisa, because of later construction and/or a renovation. Group Pise03 comes from the start of the aqueduct (cistern of Ascabo Pisano, Figure 1c), while Pise04 and Pise05, drilled from the arch, come from intermediate but close segments along its path.

A total of 179 cores were drilled from the 14 archaeomagnetic sites described above, and they were subjected to archaeointensity experiments.

3. Archaeomagnetic investigation and brick composition

The intensity experiments were carried out using three Triaxe magnetometers housed at the paleomagnetic laboratory of the Institut de Physique du Globe de Paris (IPGP), of which one belongs to the Laboratoire d'Archéologie Moléculaire et Structurale (LAMS).

The Triaxe protocol has been specially designed to take advantage of the specificities of this equipment, which allows the three magnetisation components of a small specimen

174 (less than 1 cm^3 in volume) to be measured continuously up to high temperatures, either in a
175 zero field or in a laboratory field, whose intensity and direction are controlled (Le Goff and
176 Gallet, 2004).

177 This procedure, derived from the Thellier and Thellier (1959) method, was detailed in
178 previous papers (e.g. Gallet and Le Goff 2006; Genevey et al. 2009; Hartmann et al. 2010).
179 Table 2 summarises the five heating and cooling steps involved in the Triaxe procedure,
180 which are carried out between a low temperature, T1 (between 110 °C and 150 °C), and a
181 high temperature, T2, chosen such that a large part of the natural remanent magnetization
182 (NRM) is involved. Here, T2 was fixed between 400 °C and 450 °C, as almost total
183 demagnetisation was achieved at this temperature.

184 The ancient geomagnetic field intensity is inferred from the series of measurements of
185 steps #1, #3 and #5 (with increasing temperatures) – more precisely, from the averaging of the
186 R'(Ti) data computed over the temperature range where the primary component is isolated.
187 Each R'(Ti) value is equal to the ratio, multiplied by the applied laboratory field intensity,
188 between the demagnetised fractions of NRM (step #1) and thermoremanent magnetisation
189 (TRM; step #5) between T1 and Ti, with both fractions being corrected from the thermal
190 variations of the NRM fraction still blocked at T2 (step #3) (see discussion in Le Goff and
191 Gallet 2004). When a second component is observed, the R'(Ti) data are computed from a
192 higher temperature referred to as T1' up to T2.

193 It should be emphasised that this protocol takes into account the anisotropy of the
194 thermoremanent magnetisation since the laboratory field direction is automatically chosen so
195 as to induce a TRM parallel to the original NRM (Le Goff and Gallet 2004). Additionally, it
196 was experimentally observed that the Triaxe protocol allows the cooling-rate effect to be
197 overcome when the intensity values are derived from the R'(Ti) data. This characteristic was
198 verified for different archaeological collections of various ages and origins from the Near

East, Europe, Russia and Brazil (Le Goff and Gallet 2004; Genevey et al. 2009, 2013; Hartmann et al. 2010; Hervé et al. 2017; Salnaia et al. 2017). Finally, it is worth noting that an effect of multidomain grains (if any) would be mitigated with this protocol since the laboratory magnetisation acquired from T2 is almost a full TRM.

The Triaxe results were assessed on the basis of selection criteria presented in Supplementary Table 1 (see also e.g. Genevey et al. 2016). Firstly, they allow us to judge the quality of the determination at the specimen level, checking both the directional and intensity behaviours. Two specimens per fragment must then be successfully investigated, and their results must agree within a limit of 5%. A mean value is computed at the site level when deriving from at least three different fragments, and its standard deviation must be less than 5 μT and 10% to be retained. The consistency of the results is thus tested at both the fragment and group levels. The relevance of these criteria, and those related to the selection of archaeological artefacts, was *in fine* further tested through the consistency of the intensity values obtained between sites of similar age.

For those groups of fragments successfully analysed for intensity, the magnetic mineralogy was explored through progressive thermal demagnetisation of three orthogonal isothermal remanent magnetization (IRM) acquired on cubic specimen (of side 1 cm) in high (1.5 T), medium (0.4 T) and low (0.2 T) fields (Lowrie 1990). The IRM was imparted using a MMPM10 pulse magnetiser, while the magnetisation measurements were carried out using a JR-6 spinner (Agico) magnetometer. One fragment per site was subjected to these experiments. In addition, magnetic susceptibility measurements were performed for at least two fragments per site along a heating–cooling cycle between 20 °C and a high temperature chosen close to temperature T2 considered for the Triaxe experiments (here 400 °C–450 °C). These experiments aimed to confirm the thermal stability of the magnetic mineralogy on the same temperature range involved in the intensity analysis. The measurements were performed

using a KLY-3 Kappabridge coupled to a CS3 unit (Agico). Note that in our previous studies (e.g. Hartmann et al. 2011; Genevey et al. 2016), these experiments were systematically conducted on all the fragments retained in intensity. Here, this has not been the case because the magnetic susceptibility versus temperature curves were found to be almost identical for the entire collection (see below).

Brick fragments were further analysed in the laboratory of the Archaeological Superintendence of Florence in order to define their composition. After a first description by means of a Nikon SMZ800 stereo-microscope, thin sections of about 30 μm were analysed using a Leitz Ortoluz POL polarising microscope connected to a DIGIMAT image processor in order to define their petrographic paragenesis and textures, and microanalyses were also carried out using an FEI Quanta 200 electronic microscope connected to a EDX Edax DX-4 spectrometer in order to explore the chemical composition variability.

4. Results

One important feature of this collection of brick fragments is its remarkable homogeneity in terms of paleomagnetic behaviour. This behaviour is characterised by an almost total thermal demagnetisation of the NRM at relatively low temperatures – i.e., around 400 °C–450 °C, with a single magnetization component isolated from 135°C–220°C up to the highest temperatures (Supplementary Table 2). This collection also appears to be very suitable for intensity experiments. Indeed, of the 149 fragments investigated using the Triaxe magnetometers, only 24 fragments were rejected, leading to a very good success rate of 84% (Supplementary Table 2). For 11 groups of fragments, this percentage ranges from 80% to 100% at the group level, while it is more modest, between 45% and 55%, for the other three groups. It is worth noting that these percentages refer to the fragments whose magnetisation

was strong enough in relation to the Triaxe sensitivity; 27 fragments were found to be too weakly magnetised. The retained specimens (Supplementary Table 2) possess a NRM between 30 and 700 10^{-8} A.m^2 with a NRM below 250 10^{-8} A.m^2 for 90% of the collection. For 14 fragments, failures in intensity experiments were linked to a non-ideal behaviour during the thermal treatment, as illustrated in Figure 2a by the Tosc04-04B specimen. For this specimen (and corresponding fragment), the R'(Ti) data decrease continuously all over the temperature interval investigated, although only one magnetisation component is observed (Figure 2b), which prevents the recovery of a reliable intensity of the ancient magnetic field. By contrast, the Pise04-05A specimen displays an appropriate behaviour for intensity determination, with quasi-constant R'(Ti) data observed over the temperature range where the primary component is isolated (Figures 2a,c). The other reason for rejection is related to the non-fulfilled coherence test at the fragment level (10 fragments).

The very homogeneous magnetic behaviour above is associated with an almost identical magnetic mineralogy for the whole collection of fragments (at least for the fragments successfully analysed for intensity). The three-axis IRM curves show a systematic predominance of low coercivity (<0.2 T) minerals, with unblocking temperatures ranging from 450 °C to 600 °C, which are likely to be from the magnetite family with impurities of various contents (Figure 3). The thermal demagnetisation of the 1.5-T IRM also shows the presence of a small fraction of high-coercivity minerals, likely being hematite. For some fragments, we observe a fraction of minerals with unblocking temperatures below 200 °C–250 °C and high coercivity, which probably indicates the presence of epsilon iron oxide, as recently identified by López-Sánchez et al. (2017, Figure 3). The susceptibility vs temperature curves, although providing no additional information on the magnetic mineralogy, also emphasise the homogeneity of the collection, as well as the thermal stability of the magnetic mineralogy over the temperature range used for intensity determinations (inserts in Figure 3).

This consistency in the magnetic response to all the experiments above is most probably due to the use of the same raw material.

A total of 276 specimens associated to 125 brick fragments were successfully analysed for intensity. This allowed 14 new mean well-defined intensity values (Table 1) to be derived. This is illustrated in Figure 4, where each panel displays for one group all the results obtained at the specimen level.

The homogeneity of this archaeological collection is further supported by petrographic and spectrometric measurements. The original clayey material contains silicate debris attributable to quartz in both single crystal and polycrystalline aggregate forms with a sub-angular to angular morphology. There is no addition of sandy sediments, as would be the case if the material source was along the course of the Arno River. The absence of fine silt and of well rounded clasts also militate against a supply of clay from the small quarries that were active in Pisa from at least the 13th century (Clemente 2015, 2017). On another hand, it should be noted that the huge quantity of clay necessary for the construction of the large buildings studied likely exceeded the resources of these small in-town quarries (Clemente 2015, 2017). In contrast, the quartz and the other silicate (feldspars, micas) components are typical of alluvial deposits coming from the eastern part of the Monti Pisani sedimentary succession (Carratori et al., 1991). The sharped edges and the clasts typologies suggest a short transport along small watercourses contributing to the paleo-course of the Serchio River.

All fragments have in common a red-coloured isotropic matrix due to iron oxidation, as well as recrystallisation of calcium carbonate during the thermal processes, probably resulting from the addition of limestone fragments to the clay to increase the porosity of the bricks and reduce their weight. A fine granulometry is systematically observed in the limestone clasts, which are present in variable quantities and evenly distributed in the matrix. The microanalytical investigations show the same qualitative composition. All fragments appear

to be made of clayey material fired in furnaces with excess oxygen (oxidising environment) at temperatures between ~800 °C and ~980 °C. Comparison of the textural and compositional characteristics of the bricks of Pisa with those of Calcinaia and Marti shows strong similarities, except for the quantity of the limestone clasts.

Based on the results above, we suggest that the bricks used in huge quantity for the construction of the studied buildings in Pisa were manufactured in the Calcinaia area, where the presence of brick kilns since the 15th century (Alberti, 2015) is documented, and where their transport to Pisa was easy thanks to the proximity of the Arno River.

5. Discussion

Our new data obtained in Tuscany are reported in Figure 5 together with the five other archaeointensity results available in Italy for the past millennium (Evans 1986; Aitken et al. 1988; Tema et al. 2010, 2013, Tema 2011, see also Figure 6 for their geographical distribution). Alone, the Tuscan data show a decreasing trend in intensity from the middle of the 12th century to c. 1500. There was then an increase until the beginning of the 17th century, followed by a decrease in intensity for about a century. At this stage, it can be noted that the two other Italian data available for the time period (1500-1700) cannot be easily reconciled with this variation pattern. This could be the case, however, for the result with the widest dating interval if its true age would lie at either extremities of that interval. In contrast, the three most recent data appear in good agreement with the direct measurements and/or the gufm1 model predictions at Pisa (Jacskon et al. 2000).

Considering the small number of Italian intensity data, Tema et al. (2013) relied on other data available within a 900 km radius around Viterbo (central Italy) to construct an intensity variation curve for the Italian peninsula. This curve is composed of two segments, the ages of which range between 100BC and AD 400, and AD 1300 and AD 1800,

respectively. These two intervals are those where the data selected on the basis of quality criteria are sufficiently numerous. Interestingly, for the period of 1300–1800, the Italian curve is in fact largely determined from the data obtained in the south of France (e.g. Genevey et al. 2009). For this reason, to compare our new Tuscan data with the other results available regionally, we preferred to move the reduction site to an intermediate city between Paris and Pisa and then to integrate into this comparison the data obtained within a 700 km radius around this new reduction site. Here, we chose Beaune in the Burgundy region, home to the famous Hôtel-Dieu de Beaune (Figure 6). Note that one of the French data, precisely dated to the mid-15th century from archival documents, has been obtained from analysis of pavement tiles from the so-called King's Room in the Hospices de Beaune (Genevey et al. 2009).

At first, we only considered our datasets (Genevey and Gallet, 2002; Genevey et al. 2009, 2013 and this study), as together they form a very homogeneous data collection from an experimental point of view (i.e., same experimental protocol and selection criteria). Their geographic distribution is shown in Figure 6 (blue and pink circles), and their intensity values reduced to the latitude of Beaune are reported in Figure 7a. We observe that they are remarkably consistent and complementary. The Tuscan data confirm some of the rapid intensity variations previously observed only from the French dataset (Genevey et al. 2009, 2013, 2016). It is worth recalling that the latter dataset showed that these variations were characterised throughout the past millennium by three peaks in intensity detected during the 12th century, the second part of the 14th century, and around AD 1600. The Tuscan data allow us to constrain the intensity maximum at the transition of the 16th and 17th centuries, with a peak that now appears better defined and more pronounced (Figure 7a). The new result dated from the middle of the 12th century is also important because it further documents the peak of intensity observed during this century, in particular the rapid decrease in intensity between c. 1150 and c. 1250.

In a second step, we also reported in Figure 7b all available data obtained within a 700 km radius of Beaune (Figure 6), which fulfil modern quality criteria (as defined by, for example, Genevey et al. 2016). We only kept data with age uncertainties of less than 100 years, considering that for this recent period of European history, it is possible to access such accurate dating when the aim is to recover rapid geomagnetic field intensity variations. Overall, the data available are very consistent. The additional data included here (Chauvin et al. 2000; Casas et al. 2005; Donadini et al. 2008; Gómez-Paccard et al. 2012) allow, in particular, a better description of intervals characterised by a decrease in intensity – i.e., during the 10th, 15th and 17th centuries.

From the data selection above, we constructed a reference intensity variation curve using the method recently developed by Livermore et al. (2018). This method relies on a trans-dimensional Bayesian approach that aims to fit a series of linear segments to the data, the number of which is self-determined by the data themselves. A great asset of this technique is the minimum regularisation imposed on the fit to the dataset (see discussion in Livermore et al., 2018). The average curve obtained, and its 95% confidence interval, is shown in Figure 7b. The results are very similar to those previously discussed by Genevey et al. (2016) and Livermore et al. (2018) using different averaging techniques, which further demonstrates the robustness of the three intensity peaks observed over the past millennium. Note that this result is particularly interesting for the attempts to find a correlation (and possible causal link) between geomagnetic field intensity peaks and cooling episodes in Western Europe as documented by advances and retreats of alpine glaciers, as well as with fluctuations in the C14 production rate (Gallet et al. 2005; Genevey et al. 2009, 2013). Furthermore, it is also worth reminding that the three intensity peaks, now better defined thanks to the new Tuscan data, are part of a set of five maxima regularly spaced since about 1500 years ago, with a pseudo period of ~250 years (Genevey et al. 2016; Livermore et al. 2018).

Moving away from the area of 700 km around Beaune or Paris, the past millennium in Europe is well documented by sets of data mainly acquired in northern Germany (Schnepp et al. 2009), Spain (Gómez-Paccard et al. 2006, 2008, 2012, 2016) and further east in Bulgaria (Kovacheva et al. 2014). Comparison between, on the one hand, these results and, on the other hand, the variations predicted in Paris from different global and regional field models (Pavón-Carrasco et al., 2009, 2014a; Korte et al., 2009; Licht et al., 2013), has already been widely discussed in our previous publications (Genevey et al. 2009, 2013, 2016; see also in Pavón-Carrasco et al., 2014b). It should be noted that extending the area around Beaune for instance to 900 km or 1000 km would lead to a dataset almost identical to that available in a radius of 1250 km around Paris (Genevey et al., 2016); we recall that in this case, the data appears significantly more scattered than the dataset available in a 700-km radius, which results in the smoothing of most of the rapid intensity variations mentioned (see Fig. 7 in Genevey et al., 2016). Redoing this comparison work would not provide new information compared to the conclusions of Genevey et al (2016) and for this reason, we chose here to perform a comparison with a new dataset obtained in Spain (Molina-Cardín et al. 2018). These authors constructed a new intensity variation curve for the Iberian Peninsula, spanning the past 3000 years, using both new data and previous results that fulfil a set of quality criteria, available in a radius of 900 km around Madrid. For the past millennium, this data selection is essentially different from the one considered around Beaune, even if some data obtained in France are common to both selections (Figure 6). Let us note that the selection criteria used by Molina-Cardín et al. (2018) are slightly less restrictive than those used to select the data reported in Figure 7b (Genevey et al. 2013). The criteria relative to the intensity methods are the same (Thellier method with pTRM-checks and TRM anisotropy effect taken into account for artefacts recognized as more anisotropic), but they differ for the dating uncertainties and data accuracy. In Molina-Cardín et al. (2018), the age uncertainties

399 are required to be of less than 250 years and there is no threshold value relative to the
400 uncertainty on the intensity mean, whereas, our selection is based on a dating accuracy of less
401 than 100 years and an uncertainty of less than 15% on the intensity mean. Applying our
402 selection criteria to the Spanish dataset would have comparatively resulted in the rejection of
403 13 data, mainly on the basis of the age uncertainties (11 of the 13 data indicated by crosses in
404 Figure 7c). Regardless of the criteria considered, the data selected around Madrid are
405 significantly more scattered than those presented in Figure 7b. A mean intensity variation
406 curve was constructed in Figure 7c using the data selection used by Molina- Cardín et al.
407 (2018). The dispersion of the data leads to a smooth evolution showing a continuous decrease
408 between c. 1100 and c. 1850, followed in continuity by the intensity decrease predicted by
409 gufm1 at Madrid since 1850 (Figure 7c). It should be noted that the very same evolution is
410 obtained when the Spanish data are selected according to our selection criteria. The same
411 overall trend is observed from the Beaune dataset, but thanks to a higher coherence between
412 the results, it allows us to detect the existence of faster intensity variations occurring on the
413 century timescale (Figure 7b). It therefore seems likely that a reduction of the scatter in the
414 Madrid dataset would allow the emergence of the same three intensity peaks observed in
415 France and partly in Italy. From this point of view, the data obtained in France and in Tuscany
416 indicate that the construction of a mean intensity variation curve with a resolution on a 100-
417 year timescale is an achievable objective, although it must be acknowledged that this is
418 clearly a difficult task.
419
420 **Acknowledgments**
421 The authors are indebted with Federico Andreazzoli for his great help for the selection of the
422 structures and on the field. Claudia Principe wants to remember here their two-voices speech
423 from the pulpit of the church of Marti about devil and archaeomagnetism. We are also pleased

to thank Fiorella Ramacogi and the late Mario Ferretti from the Soprintendenza to Monuments of Pisa, who produced us the due authorization for sampling. We are grateful to two anonymous reviewers for their helpful comments on the manuscript. This research was supported by the CNRS (Projet International de Collaboration Scientifique, PICS n°3063) and by the Simone and Cino Del Duca Foundation of the French Academy of Science (ID 100009515). This is IPGP contribution no. 4093.

References

Aitken, M. J., Allsop, A. L., Bussell, G. D., Winter, M. B., 1988. Determination of the intensity of the Earth's magnetic field during archaeological times: Reliability of the Thellier technique. Rev. Geophys. 26, 3-12.

Alberti, A., Baldassarri, M., 2004. a cura di, Dal castello alla "terra murata". Calcinaia e il suo territorio nel Medioevo, Firenze.

Alberti, A., 2015. La forace Coccapani di Calcinaia. Recupero della Memoria e musealizzazione. In. Bruni S., ed., "Rentamer le discours. Scritti per Mauro Del Corso", 39-47.

Arrighi, S., Tanguy, J.-C., Rosi, M., 2006. Eruption of the last 2200 years at Vulcano and Vulcanello (Aeolian Islands, Italy) dated by high-accuracy archaeomagnetism. Phys. Earth Planet. Inter. 159, 225-233.

Branca, S., Condomines, M., Tanguy, J., C., 2015a. Flank eruptions of Mt Etna during the Greek-Roman and Early Medieval periods: New data from Ra-226-Th-230 dating and archaeomagnetism. J. Volcanol.Geothermal. Res., 304, 265-271, DOI: 10.1016/j.jvolgeores.2015.09.002.

447 Branca, S., Coltelli, M., Groppelli, G., 2015b. Geological Map of Etna Volcano, with
448 contributions of Carbone, E., Lentini, F., De Beni, E., Tanguy, J.-C., Wijbrans, J. R.,
449 Memorie descrittive della carta geologica d'Italia, XCVIII.

450 Carratori, L., Ceccarelli Lemut, M. L., Frattarelli, F., Garzella,G., Greco, G., Grifoni
451 Cremonesi, R., Mazzanti, R., Morelli, P., Nencini, C., Pasquinucci, M., Pescaglini
452 Monti, R., Pult Quaglia, A.M., Rau, A., Ronzani, M., Tozzi, C., 1991. Carta 1:50.000
453 degli elementi naturalistici e storici della pianura di Pisa e dei rilievi contermini.
454 CSGDSA-CNR e Provincia di Pisa, SELCA. In "La Pianura di Pisa ed i rilievi
455 contermini. La natura e la storia", Renzo Mazzanti (a cura di), Roma, Memorie della
456 Società Geografica Italiana, vol. L, 1994.

457 Casas, L., Shaw, J., Gich, M., Share, J. A., 2005. High-quality microwave archaeointensity
458 determinations from an early 18th century AD English brick kiln. Geophys. J. Int., 161,
459 653–661.

460 Chauvin, A., Garcia, Y., Lanos, P., Laubenheimer, F., 2000. Paleointensity of the
461 geomagnetic field recovered on archaeomagnetic sites from France. Phys. Earth
462 Planet. Inter., 120, 111–136.

463 Clemente G., 2015, Fornaci da mattoni e fornaciai a Pisa tra XV e XVI secolo attraverso le
464 fonti documentarie, in Luongo. A., Paperini M., 2015, a cura di, Medioevo in
465 Formazione, III. Studi storici e multidisciplinarietà, Livorno, pp. 151-157.

466 Clemente G. 2017, Ceramisti e produzione ceramica a Pisa tra Medioevo ed età Moderna, in
467 'Ricerche Storiche', XLVI/3, 2016, pp. 133-145.

468 Ciuti, R., 2003. Pisa Medicea. Itinerario Storico Artistico tra Cinquecento e Seicento, Pisa.

469 Donadini, F., Pesonen, L.J., 2007. Archaeointensity determinations from Finland, Estonia,
470 and Italy. Geophysica, 43(1-2), 3-18.

471 Donadini, F., Kovacheva, M., Kostadinova, M., Hedley, I.G., Pesonen, L.J., 2008.
472 Palaeointensity determination on an early medieval kiln from Switzerland and the
473 effect of cooling rate. Phys. Earth. Planet. Inter., 33, 449–457.

474 Evans, M.E., 1986. Paleointensity estimates from Italian kilns. J. Geomagn. Geoelect. 38,
475 1259–1267.

476 Evans, M.E., 1991. An archaeointensity investigation of a kiln at Pompeii. J. Geomagn.
477 Geoelect. 3843(5), 357-361.

478 Febbraro, M., 2006. La pieve di S. Maria Novella di Marti. Spunti interpretativi per una
479 conoscenza dell'architettura in laterizi nel Valdarno inferiore, in Baldassarri M.,
480 Ciampoltrini G. 2006, a cura di, I Maestri dell'Argilla. L'edilizia in cotto, la
481 produzione di laterizi e di vasellame nel Valdarno Inferiore tra Medioevo ed età
482 Moderna, Pisa, pp. 51-64.

483 Gallet, Y., Genevey, A., Fluteau, F., 2005. Does Earth's magnetic field secular variation
484 control centennial climate change?, Earth Planet. Sci. Lett., 236, 339–347.

485 Gallet, Y., Le Goff, M., 2006. High-temperature archaeointensity measurements from
486 Mesopotamia. Earth Planet. Sci. Lett. 241, 159-173.

487 Gallet, Y., Genevey, A., Le Goff, M., Warmé, N., Gran-Aymerich, J., Lefèvre, A., 2009. On
488 the use of archaeology in geomagnetism, and vice-versa: Recent developments in
489 archaeomagnetism. C. R. Physique, 10 630–648.

490 Gasperini, M., Greco, G., Noferi, M., Tagliagamba, S., 2015. a cura di, Il Principe, la città,
491 l'acqua. L'acquedotto mediceo di Pisa, Pisa.

492 Gattiglia, G., Milanese, M., 2006. Palazzo Scotto Corsini. Archaeologia e storia delle
493 trasformazioni di un'area urbana a Pisa tra XI e XX secolo, Pisa.

494 Genevey, A., Gallet, Y., 2002. Intensity of the geomagnetic field in western Europe over the
495 past 2000 years: new data from ancient French pottery. J. Geophys. Res. 107 (B11),
496 doi:10.1029/2001JB000701.

497 Genevey, A., Gallet, Y., Constable, C. G., Korte, M., Hulot, G., 2008. ArchaeoInt: An
498 upgraded compilation of geomagnetic field intensity data for the past ten millennia and
499 its application to the recovery of the past dipole moment. Geochem. Geophys.
500 Geosyst., 9, Q04038, doi:10.1029/ 2007GC001881.

501 Genevey, A., Gallet, Y., Rosen, J., Le Goff, M., 2009. Evidence for rapid geomagnetic field
502 intensity variations in Western Europe over the past 800 years from new
503 archaeointensity French data. Earth Planet. Sci. Lett. 284, 132-143.

504 Genevey, A., Gallet, Y., Thébault, E., Jesset, S., Le Goff, M., 2013. Geomagnetic field
505 intensity variations in Western Europe over the past 1100 years. Geochem. Geophys.
506 Geosyst. 14/8, 2858-2872.

507 Genevey, A., Gallet, Y., Jesset, S., Thébault, E., Bouillon, J., Lefèvre, A., Le Goff, M., 2016.
508 New archaeointensity data from French Early Medieval ceramic production (6th-10th
509 century AD). Tracing 1500 years of geomagnetic field intensity variations in Western
510 Europe. Phys. Earth Planet. Inter. 257, 205-219.

511 Gómez-Paccard, M., Chauvin, A., Lanos, P., Thiriot, J., Jiménez-Castillo, P., 2006.
512 Archaeomagnetic study of seven contemporaneous kilns from Murcia (Spain). Phys.
513 Earth Planet. Inter., 157, 16–32.

514 Gómez-Paccard, M., Chauvin, A., Lanos, P., Thiriot, J., 2008. New archaeointensity data
515 from Spain and the geomagnetic dipole moment in western Europe over the past 2000
516 years. J. Geophys. Res., 113, B09103, doi:10.1029/2008JB005582.

Gómez-Paccard, M., Chauvin, A., Lanos, P., Dufresne, P., Kovacheva, M., Hill, M. J., Beamud, E., Blain, S., Bouvier, A., Guibert, P., and Archaeological Working Team, 2012. Improving our knowledge of rapid geomagnetic field intensity changes observed in Europe between 200 and 1400 AD. Earth Planet. Sci. Lett., 355-356, 131–143.

Gómez-Paccard, M., Osete, M. L., Chauvin, A., Pavón-Carrasco, F. J., Pérez-Asensio, M., Jiménez, P., Lanos, P., 2016. New constraints on the most significant paleointensity change in Western Europe over the last two millennia. A non-dipolar origin? Earth Planet. Sci. Lett., 454, 55–64.

Hartmann, G., Genevey, A., Gallet, Y., Trindade, R., Etchevarne, C., Le Goff, M., Afonso, M., 2010. Archaeointensity in Northeast Brazil over the past five centuries. Earth Planet. Sci. Lett. 296, 340-352.

Hartmann, G., Genevey, A., Gallet, Y., Trindade, R., Le Goff, M., Najjar, R., Etchevarne, C., Afonso, M., 2011. New historical archaeointensity data from Brazil : Evidence for a large regional non-dipole field contribution over the past few centuries. Earth Planet. Sci. Lett. 306, 66-76.

Hedley, I., Wagner, G.C., 1991. A magnetic investigation of roman andpre-roman pottery, in Archaeometry ’90 pp. 275–284, eds Pernicka, E. &Wagner, G.C., Birkhäuser verlag, Basel.

Hervé, G., Fassbinder, J., Gilder, S., Metzner-Nebelsick, C., Gallet, Y., Genevey, A., Schnepp, E., Geisweid, L., Pütz, A., Reub, S., Wittenborn, F., Flontas, A., Linke, R., Riedel, G., Walter, F., Westhausen, I., 2017. Fast geomagnetic field intensity variations between 1400 and 400 BCE: new archaeointensity data from Germany. Phys. Earth Planet. Inter. 270, 143–156.

Hill, M., Lanos, P., Chauvin, A., Vitali, D., Laubenheimer, F., 2007. An archaeomagnetic investigation of a Roman amphorae workshop in Albinia (Italy). Geophys. J. Int. 169, 471-482.

Hill, M.J., Lanos, P., Denti, M., Dufresne, P., 2008. Archaeomagnetic investigation of bricks from the VIIIth–VIIth century BC Greek–indigenous site of Incoronata (Metaponto, Italy). Phys. Chem. Earth 33, 523-533.

Jackson, A., Jonkers, A., Walker M., 2000. Four centuries of geomagnetic secular variation from historical records. Philos. Trans. R. Soc. London Ser. A 358, 957– 990.

Kapper, L., Anesin, D., Donadini, F., Angelucci, D., Cavulli, F., Pedrotti, A., Hirt, A., 2014, Linking site formation processes to magnetic properties. Rock- and archaeomagnetic analysis of the combustion levels at Riparo Gaban (Italy), J. Arch. Sci., 41, 836–855.

Kovacheva, M., Kostadinova-Avramova, M., Jordanova, N., Lanos, Ph., Boyadzhiev, Y., 2014. Extended and revised archaeomagnetic database and secular variation curves from Bulgaria for the last eight millennia. Phys. Earth Planet. Inter., 236, 79–94.

Korte, M., Donadini, F., Constable, C. G., 2009. Geomagnetic field for 0–3 ka: 2. A new series of time-varying global models. Geochem. Geophys. Geosyst., 10, Q06008, doi:10.1029/2008GC002297.

Le Goff, M., Gallet, Y., 2004. A new three-axis vibrating sample magnetometer for continuous high-temperature magnetization measurements: applications to paleo- and archaeo-intensity determinations. Earth Planet. Sci. Lett. 229, 31-43.

Licht, A., Hulot, G., Gallet, Y., Thébault, E., 2013. Ensembles of low degree archaeomagnetic field models for the past three millennia. Phys. Earth. Planet. Inter., 224, 38–67.

562 Livermore, P. W., Fournier, A., Gallet, Y., 2014. Core-flow constraints on extreme
563 archaeomagnetic intensity changes. Earth Planet. Sci. Lett., 387, 145–156,
564 doi:10.1016/j.epsl.2013.11.020.

565 Livermore, P.W., Fournier, A., Gallet, Y., Bodin, T., 2018. Transdimensional inference of
566 archaeomagnetic intensity change. Geophys. J. Int. 215, 2008-2034.

567 López-Sánchez, J., McIntosh, G., Osete, M.L., del Campo, A., Villalain, J.J., Pérez, L., M.
568 Kovacheva, M., Rodriguez de la Fuente, O., Epsilon iron oxide: Origin of the high
569 coercivity stable low Curie temperature magnetic phase found in heated archaeological
570 materials, Geochem. Geophys. Geosyst. 18, 2646-2656.

571 Lowrie, W., 1990. Identification of ferromagnetic minerals in a rock by coercivity and
572 unblocking temperatures properties. Geophys. Res. Lett., 17, 159–162.

573 Malfatti, J., Principe, C., Gattiglia, G., 2011. Archaeomagnetic Directional Investigation of a
574 Metallurgical Furnace in Pisa (Italy). Journal of Cultural Heritage; vol 12, 2011, 1-10.

575 Molina-Cardín, A., Campuzano, S. A., Osete, M. L., Rivero-Montero, M., Pavón-Carrasco, F.
576 J., Palencia-Ortas, A., Martín-Hernández, F., Gómez-Paccard, M., Chauvin, A.,
577 Guerrero-Suárez, S., Pérez-Fuentes, J. C., McIntosh, G., Catanzariti, G., Sastre Blanco,
578 J. C., Larrazabal, J., Fernández Martínez, V. M., Álvarez Sanchís, J. R., Rodríguez-
579 Hernández, J., Martín Viso, I., Garcia i Rubert, D., 2018. Updated Iberian
580 Archaeomagnetic Catalogue: New Full Vector Paleosecular Variation Curve for the
581 Last Three Millennia. Geochem. Geophys. Geosyst., 19, 10, 3637-3656.

582 Paolillo, A., Principe, C., Bisson, M., Gianardi, R., Giordano, D., La Felice, S., 2016.
583 Volcanology of the South-Western sector of Vesuvius, Italy. Journal of Maps, 12, 425-
584 440, DOI 10.1080/17445647.2016.1234982.

585 Pavón-Carrasco, F. J., Osete, M. L., Torta, J. M., Gaya-Piqué, L. R., 2009. A regional
586 archaeomagnetic model for Europe for the last 3000 years, SCHA.DIF.3K:
587 Applications to archaeomagnetic dating. Geochem. Geophys. Geosyst., 10, Q03013,
588 doi:10.1029/2008GC002244.

589 Pavón-Carrasco, F. J., Osete López, M. L., Torta, J. M., De Santis, A., 2014a. A geomagnetic
590 field model for the Holocene based on archaeomagnetic and lava flow data. Earth
591 Planet. Sci. Lett., 388, 98–109.

592 Pavón-Carrasco, F. J., Gómez-Paccard, M., Hervé, G., Osete López, M. L., Chauvin, A.,
593 2014b. Intensity of the geomagnetic field in Europe for the last 3 ka: Influence of data
594 quality on geomagnetic field modelling. Geochem. Geophys. Geosyst., 15, 2515-2530,
595 doi:10.1002/2014GC00531.

596 Principe, C., Tanguy, J.C., Arrighi, S., Paiotti, A., Le Goff, M., Zoppi, U., 2004. Chronology
597 of Vesuvius' activity from A.D. 79 to 1631 based on archaeomagnetism of lavas and
598 historical sources, Bull. Volcanol. 66,703–724.

599 Principe, C., Gogichaishvili, A., Arrighi, S., Devidze, M., Le Goff, M., La Felice, S., Paolillo,
600 S., Giordano D., Morales, J., 2018. Archaeomagnetic dating of Copper Age furnaces at
601 Croce di Papa village and relations on Vesuvius and Phlegraean Fields volcanic
602 activity. Journal of Volcanology and Geothermal Energy, 349 (2018) 217–229

603 Quiros Castillo, J.A. 1997. La mensiocronologia dei laterizi della Toscana: problematiche e
604 prospettive della ricerca. In: *Archaeologia dell'Architettura*, *II*, pp. 159–166.

605 Salnaia, N., Gallet, Y., Genevey, A., Antipov, I., 2017. New archaeointensity data from
606 Novgorod (North-Western Russia) between c. 1100 and 1700 AD. Implications for the
607 European intensity secular variation. Phys. Earth Planet. Inter. 269, 18-28.

608 Schnepp, E., Lanos, P., Chauvin, A., 2009. Geomagnetic paleointensity between 1300 and
609 1750 A.D. derived from a bread oven floor sequence in Lübeck, Germany. Geochem.
610 Geophys. Geosyst., 10, Q08003, doi:10.1029/2009GC002470.

611 Sodi, S., Radi, A., 1979. L'Oratorio di S. Bernardino e la sua confraternita, Pisa.

612 Sodi, S., Renzoni, S., 2003. La chiesa di Santo Stefano e la piazza dei Cavalieri, Pisa.

613 Tanguy, J.-C., Le Goff, M., Chillemi, V., Paiotti, A., Principe, C., La Delfa, S., Patanè, G,
614 1999. Secular variation of the geomagnetic field direction recorded in lavas from Etna
615 and Vesuvius during the last two millennia. C.R. Acad. Sci., Series IIA, Earth and
616 Planetary Sciences, 329, 557-564.

617 Tanguy, J.C., LeGoff, M., Principe, C., Arrighi, S., Chillemi, V., Paiotti, A., LaDelfa, S.,
618 Patanè, G., 2003. Archaeomagnetic dating of Mediterranean volcanics of the last 2100
619 years: validity and limits. Earth Planet. Sci. Lett. 211, 111–124.

620 Tanguy, J.-C., Condomines, M., Le Goff, M., Chillemi, V., La Delfa, S., Patanè, G., 2007.
621 Mount Etna eruptions of the last 2,750 years: revised chronology and location through
622 archaeomagnetic and ^{226}Ra-^{230}Th dating. Bull. Volcanol. 70, 55-83.

623 Tanguy, J., C., Condomines, M., Branca, S., La Delfa, S., Coltelli, M., 2012, New
624 archaeomagnetic and Ra-226-Th-230 dating of recent lavas for the Geological map of
625 Etna volcano. It. J. Geosc., 131, 2, 241-257, DOI: 10.3301/IJG.2012.01.

626 Tema E., Hedley, I. and Lanos, P., 2006. Archaeomagnetism in Italy: a compilation of data
627 including new results and a preliminary Italian secular variation curve. *Geophys. J.*
628 *Int.*, 167, 1160-1171.

629 Tema, E., Goguitchaichvili, A., Camps, P., 2010. Archaeointensity determination from Italy:
630 new data and Earth's magnetic field strength variation over the past three millennia.
631 Geophys. J. Int.180, 596–608.

632 Tema, E., 2011. Archaeomagnetic Research in Italy: Recent achievements and future
633 perspectives. In: *The Earth's Magnetic Interior*, IAGA Special Sopron Book Series,
634 Volume 1, Chapter 15, pp. 213-233. Eds: Petrovsky, E., Herrero-Bervera, E.,
635 Harinarayana, T., Ivers, D., Springer.

636 Tema, E., Morales, J., Goguitchaichvili, A., Camps, P., 2013. New archaeointensity data from
637 Italy and geomagnetic field intensity variation in the Italian Peninsula. Geophys. J. Int.
638 193, 603–614.

639 Tema, E., Camps, P., Ferrara, E., Poidras, T., 2015. Directional results and absolute
640 archaeointensity determination by the classical Thellier and the multi-specimen DSC
641 protocols for two kilns excavated at Osterietta, Italy, Stud. Geophys. Geod., 59, DOI:
642 10.1007/s11200-015-0413-0.

643 Tema, E., Ferrara, E., Camps, P., Conati Barbaro, C., Spatafora, S., Carvallo, C., Poidras, T.,
644 2016. The Earth's magnetic field in Italy during the Neolithic period: New data from
645 the Early Neolithic site of Portonovo (Marche, Italy). Earth Planet. Sci. Lett. 448, 49-
646 61.

647 Thellier, E., Thellier, O., 1959. Sur l'intensité du champ magnétique tesrrestre dans le passé
648 historique et géologique. Ann. Géophys. 15, 285-376.

649 Vezzoli, L., Principe, C., Malfatti, J., Arrighi, S., Tanguy, J.C., Le Goff, M., 2009. Modes and
650 times of caldera resurgence: The <10 ka evolution of Ischia Caldera, Italy, from
651 archaeomagnetic dating. Journal Volcanol Geotherm Res, 186, 305-319.

652

653 **Figure and Table captions**

654

655 Figure 1: Examples of Tuscan baked-brick buildings sampled for this archaeointensity study.

(a) ‘Bocchette di Putignano’. This dike was built in 1558 as indicated on a plaque affixed to the building (b), which reads ‘A PARTV VIRGINIS ANNO M. D. LVIII. CALEN. NOVEMBRIS’ and can be translated as ‘November 2nd of the 1558th year since the date Mary gave birth [to Jesus]’. (c) Cistern of the Medici aqueduct linking Pisa to Asciano Pisa dated from the beginning of the 17th century. The yellow cross indicates the area selected for the sampling carried out using drilling. For this site, 12 cores were collected, leaving as many visible holes (d), which were then filled with tinted mortar to restore the wall as much as possible (e).

Figure 2: Examples of favourable (Pise04-05A) and unfavourable (Tosc04-04B) magnetic behaviour for intensity determination. (a) Diagram showing the evolution of the R’(Ti) data over the temperature range investigated. (b) and (c) Corresponding thermal demagnetisation diagrams. Only one magnetisation component is observed in both cases. For the specimen Pise04-05A, the R’(Ti) data are almost constant and their mean provides a reliable intensity value. The decrease in the R’(Ti) data over the entire temperature range observed for the specimen Tosc04-04B indicates a varying proportionality between the NRM and TRM fractions, thereby invalidating the possibility of recovering the ancient magnetic field intensity for this brick fragment.

Figure 3: Characterisation of the magnetic mineralogy. Typical example of thermal demagnetisation of three-axis IRM acquired in fields of 1.5, 0.4 and 0.2 T. The inserts show the low field susceptibility vs temperature curves for the corresponding fragments (heating/cooling in black/grey).”.

Figure 4: Intensity results obtained for four groups of brick fragments. Each curve in the different panels represents the evolution of the R'(Ti) data for one specimen over the temperature range considered for intensity determination. There are 80 determinations, corresponding to as many specimens, represented here. This figure makes it possible to assess the consistency of the results obtained at the fragment and group levels

Figure 5: New archaeointensity data obtained in Pisa and its neighbouring territory, and their comparison with the other archaeointensity results available in Italy for the past millennium, the direct measurements and the intensity values expected in Pisa from the gufm1 model (Jackson et al. 2000) from 1850 onwards. All data were reduced to the latitude of Pisa.

Figure 6: Geographical distribution of the Italian archaeointensity data (pink circles, the new Tuscan data; purple squares, previously acquired data), the dataset previously acquired in France and Belgium (blue points; Genevey et al. 2009, 2013) and the other data selected (green squares) within 700 km around Beaune (purple circle) and within 900 km around Madrid (yellow circle; Molina-Cardín et al. 2018).

Figure 7: Archaeointensity variations in Western Europe over the past millennium as inferred from different data selections (a) New Tuscan data, together with other results previously acquired in France and Belgium (Genevey and Gallet 2002; Genevey et al. 2009, 2013) and from direct measurements (http://www.bcmt.fr/). (b) Intensity data fulfilling quality criteria and available within 700 km around Beaune, and mean geomagnetic field intensity variation curve, and its 95% confidence envelope, computed from this dataset using the AH-RJMCMC algorithm developed by Livermore et al. (2018). The computational parameters are as follows: $\sigma_{move} = 200$ yr, $\sigma_{change} = 15\ \mu$T, $\sigma_{birth} = 8\ \mu$T, $\sigma_{ages} = 5$ yr, $\beta = 20$, $K_{max}=80$, with a chain

length of 50 million samples and intensity priors of 30 μT for the minimum and 100 μT for the maximum (see details in Livermore et al., 2018). Following Genevey et al. (2008), the datum obtained by Casas et al. (2005) marked by '*' was decreased by 5% to account for the cooling-rate effect, which was not evaluated in this study. (c) Intensity data selected by Molina-Cardín et al. (2018) for a region of 900 km around Madrid and the corresponding mean intensity variation curve computed using the same method as in (b) and with the same computational parameters except for the intensity priors set at 25 μT for the minimum and 95 μT for the maximum. Note that the time-order relationship existing for two datasets was taken into account in these estimates. The symbol "x" indicates the thirteen data that would not have been retained if the same selection criteria as in Figure 7b had been chosen. The intensity values expected in Madrid since 1850 from the gufm1 model (Jackson et al. 2000) are also exhibited.

Table 1: New mean archaeointensity values obtained from the fourteen Tuscan groups of architectural brick fragments analysed in the present study. 'location' indicates the city where the brick fragments were sampled. Note, however, that the study carried out on the composition of the bricks suggests the same production area around Calcinaia (43.68°N ; 10.61°E). '# Group' indicates the archaeomagnetic identification number of each group; 'N Frag. (n Spec)' gives, respectively, the number of fragments and specimens retained to estimate a mean; 'F ± σ F (μT)' corresponds to the mean value obtained at the sampling site with its standard deviation in μT. Its reduction at the latitude of Beaune (47.02°N) is given in μT in the last column.

Table 2: Sequence of the five series of measurements involved in the Triaxe intensity protocol. The measurements are carried out every 5° C (Le Goff and Gallet, 2004).

730

731 Supplementary Table 1: Summary of the selection criteria used to retain the intensity results
732 at the specimen, fragment and group levels.

733

734 Supplementary Table 2: Intensity results obtained at the specimen level and mean values
735 obtained at the fragment level. 'Tmin-Tmax': Interval of temperature involved for the
736 intensity computation. 'Flab': Intensity of the laboratory field in μT. 'NRM T1 (T1')'
737 column: Percentage of magnetisation fraction with unblocking temperatures larger than T1 (or
738 T1'). 'Slope R': Slope of the straight line computed from the R'(Ti) data between Tmin and
739 Tmax. 'F Triaxe': Intensity values obtained at the specimen level in μT. 'F Triaxe mean value
740 per fragment $\pm$ σ F': Mean intensity value obtained at the fragment level with its standard
741 error when computed from 2 values or its standard deviation when computed from 3 values.
742 *: (n1/n2/n3) indicates successively the number of fragments collected, the number of
743 fragments whose magnetization was strong enough relative to the Triaxe sensitivity and the
744 number of fragments retained to estimate a mean value at the group level.

a)

b)

c)

d)

e)

Figure 1.

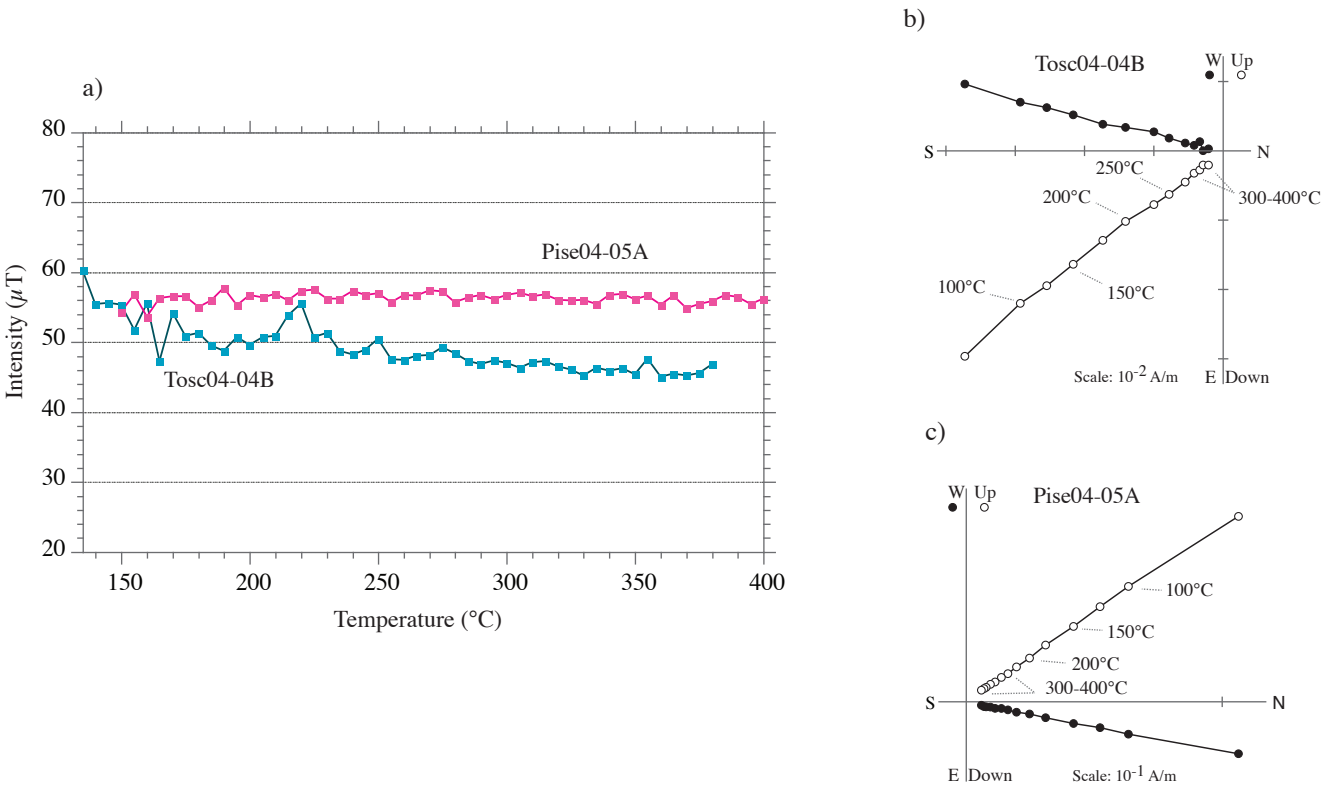
a)
80
70
60
50
40
30
20
Intensity (μT)
150
200
250
300
350
400
Temperature (°C)
Pise04-05A
Tosc04-04B
b)
Tosc04-04B
W
Up
S
N
250°C
200°C
300-400°C
100°C
150°C
Scale: 10-2 A/m
E
Down
c)
W
Up
Pise04-05A
100°C
150°C
200°C
300-400°C
S
N
E
Down
Scale: 10-1 A/m

Figure 2.

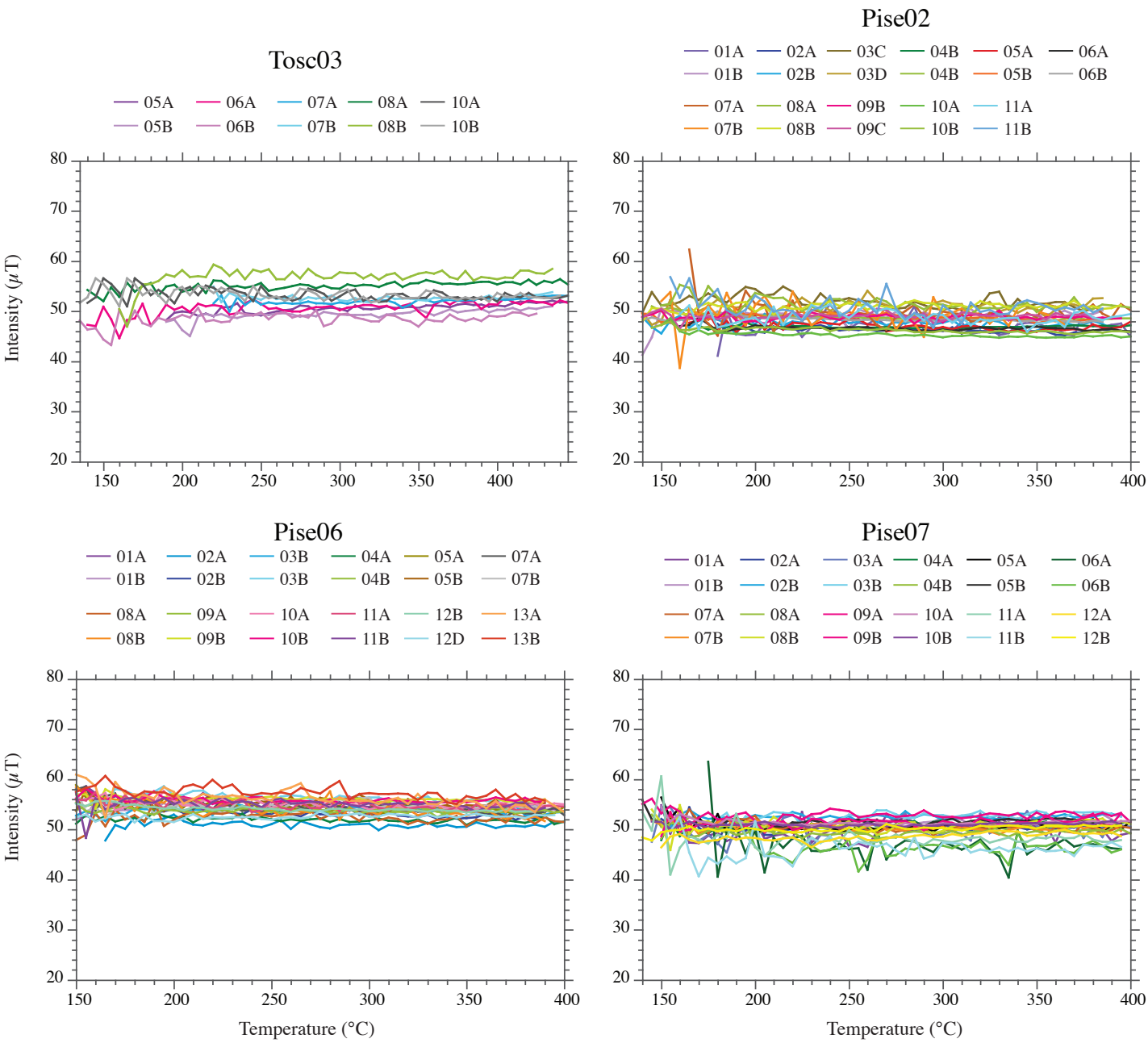
Tosc03
05A 06A 07A 08A 10A
05B 06B 07B 08B 10B
Pise02
01A 02A 03C 04B 05A 06A
01B 02B 03D 04B 05B 06B
07A 08A 09B 10A 11A
07B 08B 09C 10B 11B
Pise06
01A 02A 03B 04A 05A 07A
01B 02B 03B 04B 05B 07B
08A 09A 10A 11A 12B 13A
08B 09B 10B 11B 12D 13B
Pise07
01A 02A 03A 04A 05A 06A
01B 02B 03B 04B 05B 06B
07A 08A 09A 10A 11A 12A
07B 08B 09B 10B 11B 12B
Intensity (μT)
Temperature (°C)
20 30 40 50 60 70 80
150 200 250 300 350 400

Figure 4.

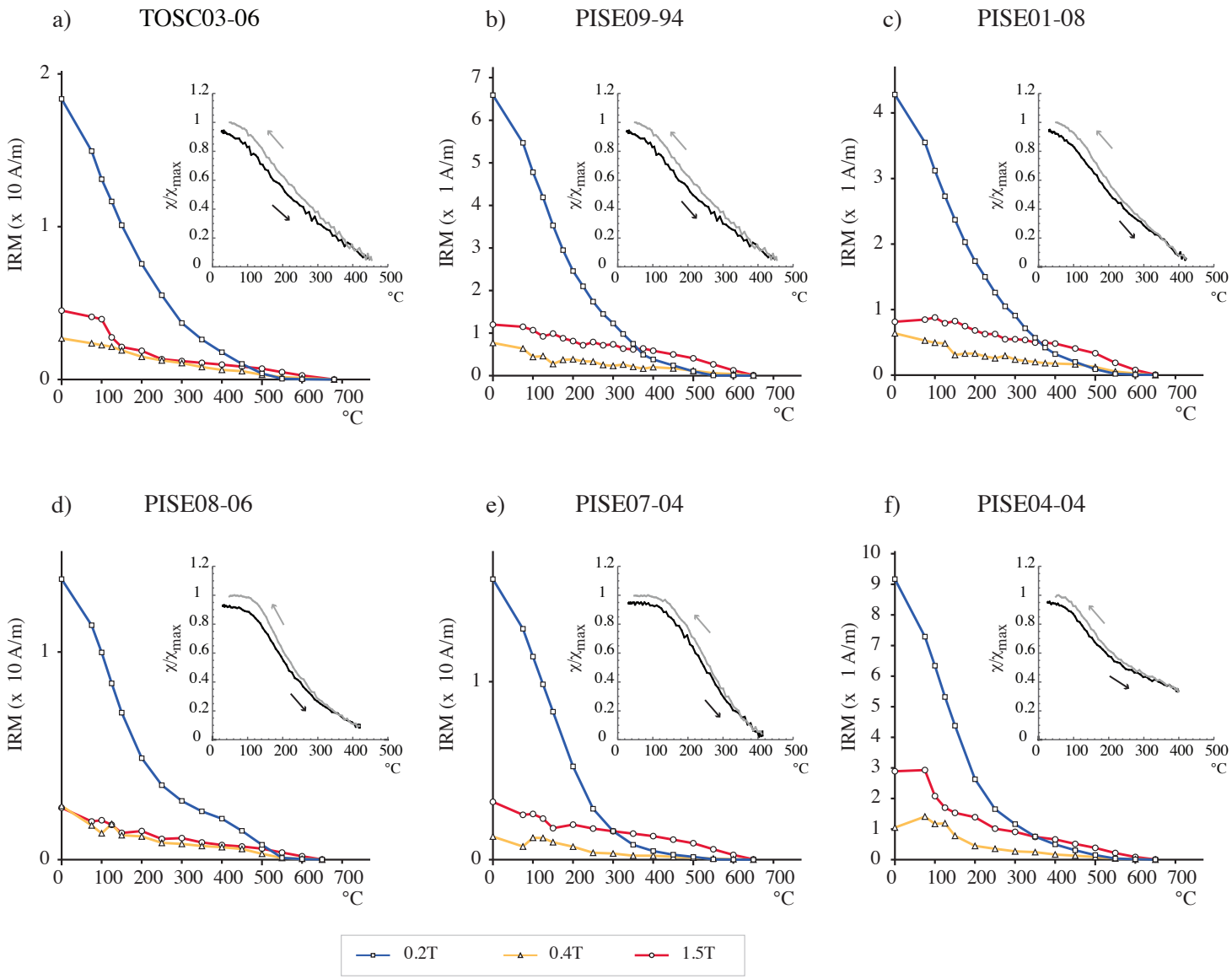
a) TOSC03-06
b) PISE09-94
c) PISE01-08
d) PISE08-06
e) PISE07-04
f) PISE04-04
IRM (x 10 A/m)
IRM (x 1 A/m)
χ/χmax
°C
0.2T
0.4T
1.5T

Figure 3.

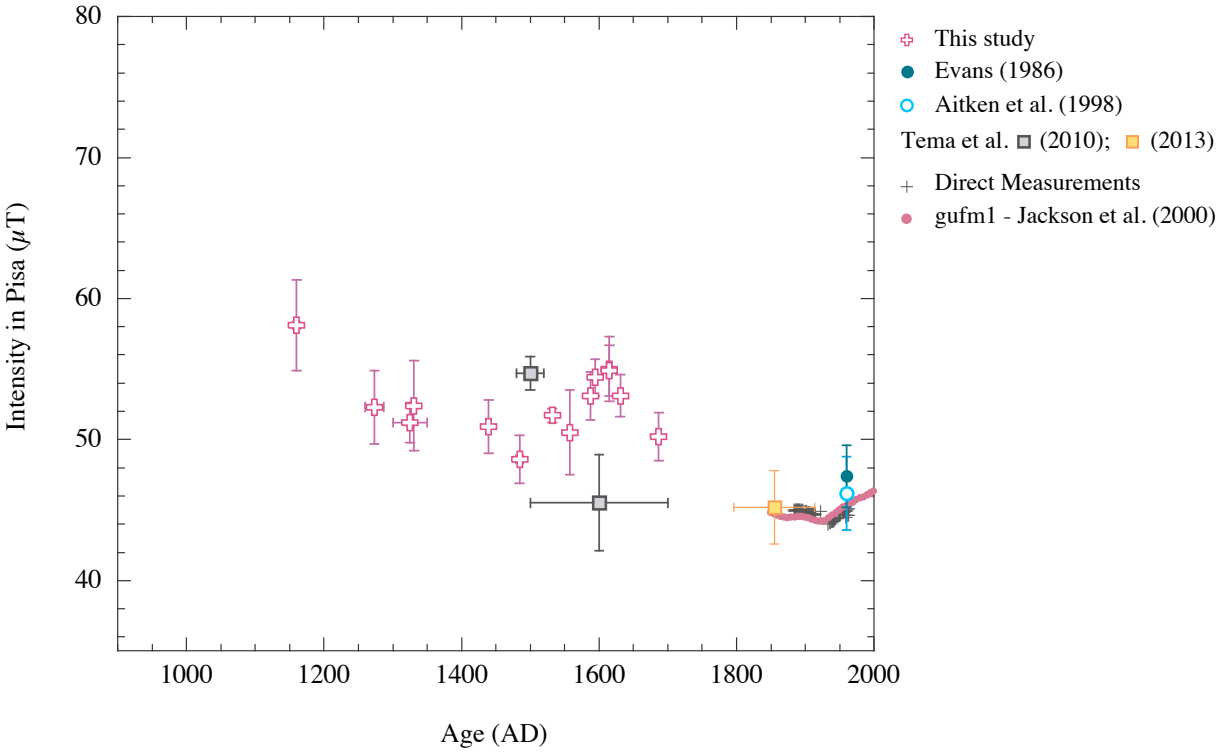
80
70
60
50
40
1000
1200
1400
1600
1800
2000
Intensity in Pisa (μT)
Age (AD)
This study
Evans (1986)
Aitken et al. (1998)
Tema et al. (2010); (2013)
Direct Measurements
gufm1 - Jackson et al. (2000)

Figure 5.

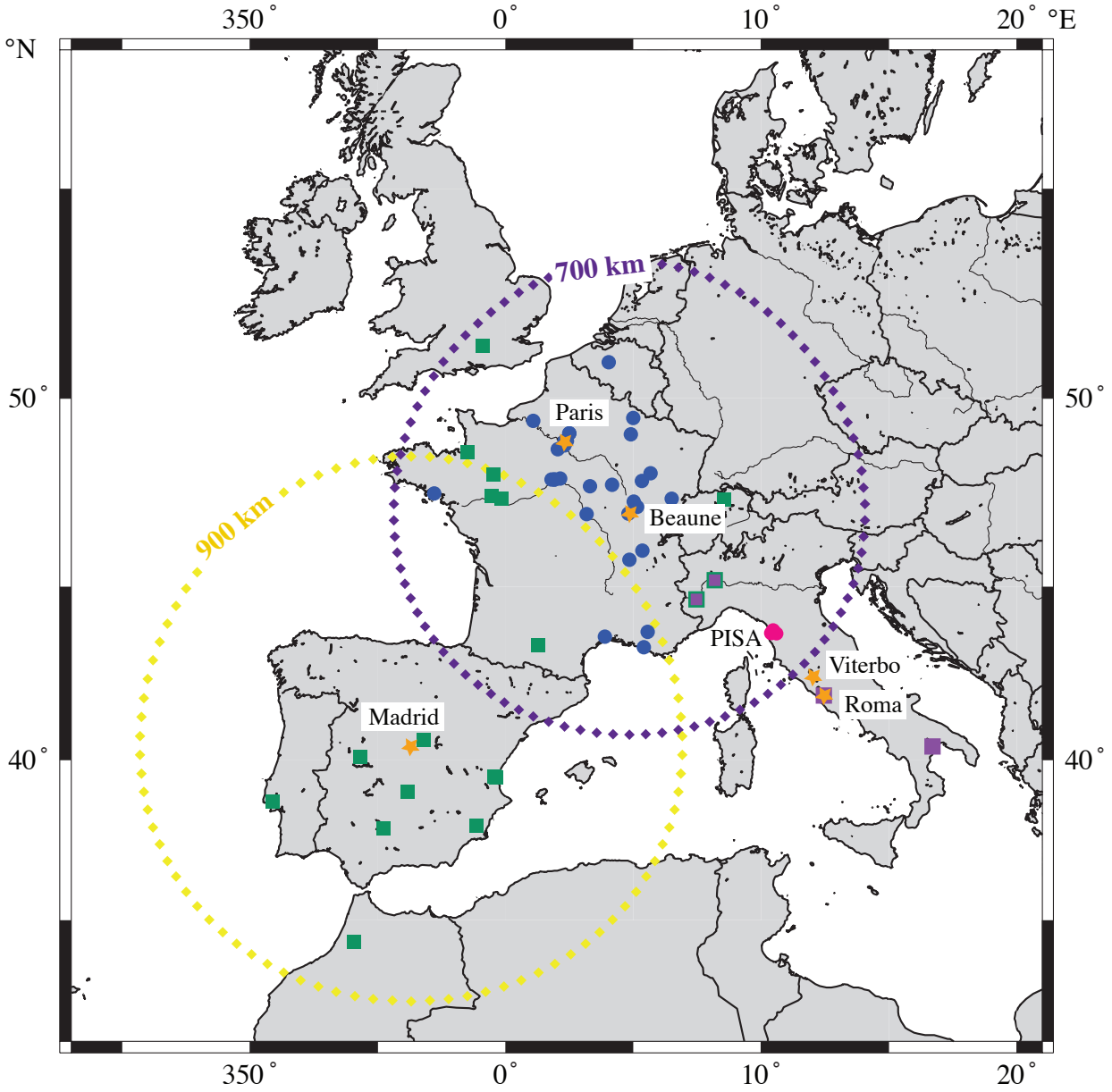
350°
0°
10°
20° °E
°N
50°
40°
700 km
900 km
Paris
Beaune
PISA
Viterbo
Roma
Madrid

Figure 6.

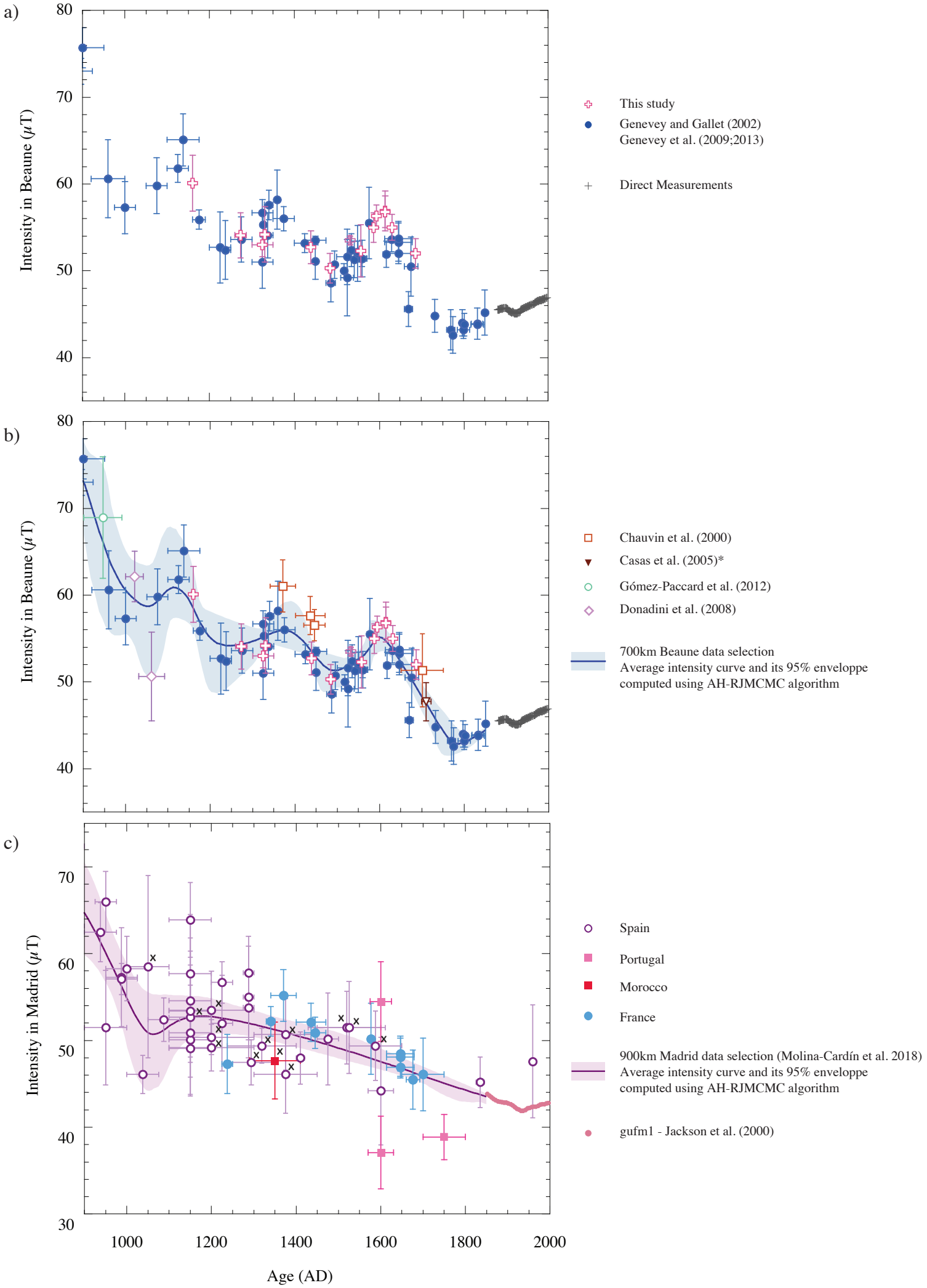
a)
b)
c)
Intensity in Beaune (μT)
Intensity in Madrid (μT)
80
70
60
50
40
30
1000
1200
1400
1600
1800
2000
Age (AD)
This study
Genevey and Gallet (2002)
Genevey et al. (2009;2013)
Direct Measurements
Chauvin et al. (2000)
Casas et al. (2005)*
Gómez-Paccard et al. (2012)
Donadini et al. (2008)
700km Beaune data selection
Average intensity curve and its 95% enveloppe
computed using AH-RJMCMC algorithm
Spain
Portugal
Morocco
France
900km Madrid data selection (Molina-Cardín et al. 2018)
Average intensity curve and its 95% enveloppe
computed using AH-RJMCMC algorithm
gufm1 - Jackson et al. (2000)

Figure 7.

Location	# Group	Age (A.D.)	Sampled baked-brick buildings	N Frag. (n Spec.)	F ± σF (μT)	at Beaune (μT) (47.02°N; 4.84°E)
Pisa	Pise12	1155-1165	Medieval walls - Scotto Garden	N = 10 (n = 29)	58.1±3.2	60.2
(43.71°N ; 10.40°E)	Pise11	1300-1350	Medieval walls - Second phase - Scotto Garden	N = 4 (n = 12)	51.2±1.4	53.0
	Pise10	1440	New citadel - Santa Barbara tower	N = 15 (n = 30)	50.9±1.9	52.7
	Pise02	1479-1490	Oratory of San Bernardino	N = 11 (n = 22)	48.6±1.7	50.3
	Pise09	1531-1533	New Citadel - Sangallo bastion	N = 5 (n = 15)	51.7±0.5	53.5
	Pise01	1558	Bocchette di Putignano	N = 3 (n = 9)	50.5±3.0	52.3
	Pise08	1588	Medici shipyard (Arsenal)	N = 6 (n = 12)	53.1±1.7	55.0
	Pise06	1595	Medici Aqueduct - Arch	N = 12 (n = 24)	54.4±1.3	56.3
	Pise07	1683-1691	Santo Stefano dei Cavalieri church - Extension of the church	N = 12 (n = 24)	50.2±1.7	52.0
Asciano Pisano	Pise03	1613-1617	Medici Aqueduct - Cistern	N = 10 (n = 20)	55.0±1.8	56.9
(43.75°N ; 10.47°E)	Pise04	1613-1617	Medici Aqueduct - Pillar	N = 9 (n = 22)	54.9±2.3	56.8
	Pise05	1632	Medici Aqueduct - Pillar	N = 13 (n = 26)	53.1±1.6	55.0
Calcinaia	Tosc03	1260-1287	Del Castello tower	N = 5 (n = 10)	52.3±2.6	54.1
(43.68°N ; 10.61°E)						
Marti	Tosc04	1331	Santa Maria Novella church	N = 10 (n = 21)	52.4±3.2	54.3
(43.65°N ; 10.74°E)						

Table 1.

Step

#1	Heating	from T1	to T2	in zero field	=> Demagnetization of the NRM
#2	Cooling	from T2	to T1	in zero field	
#3	Heating	from T1	to T2	in zero field	=> Control of the thermal variation on the magnetization fraction remaining unblocked at T2
#4	Cooling	from T2	to T1	in field	=> Acquisition of a laboratory TRM parallel to the NRM
#5	Heating	from T1	to T2	in zero field	=> Demagnetization of the laboratory TRM

Table 2.

■ Specimen level	•Thermal demagnetization	=> Well defined primary component isolated between Tmin≥T1 and Tmax=T2
	•Intensity determination	=> Performed on the temperature range [Tmin-Tmax], where the primary component is isolated
		=> Percentage of magnetization fraction with unblocking temperatures larger than Tmin ≥50%
		=> Slope of the straight line computed between the R' values at Tmin and Tmax ≤ 10% This tests the constancy of the R '(Ti) ratios on the [Tmin-Tmax] temperature range considered

■ Fragment level	=> At least n specimens ≥2
	=> Standart error (or standard deviation when n≥3) around the mean ≤ 5%

■ Site level	=> At least N fragments ≥3
	=> Standart deviation around the mean ≤ 5μT and ≤ 10%

Fragment	Specimen	T_{min}-T_{max} (°C)	F_{Lab} (μT)	NRM T1 (T1') (%)	Slope R' (%)	F Triaxe (μT)	F Triaxe mean value per fragment ± σF (μT)
Pise12, Pisa, Medieval walls, [1155-1165] AD, (12/11/10)*							
Pise12-02	Pise12-02A	165-390	50	79	4	57.3	58.6±1.2
	Pise12-02C	160-395	55	82	-2	59.3	
	Pise12-02D	155-395	55	84	-2	59.3	
Pise12-03	Pise12-03A	170-370	50	79	-3	60.0	61.3±1.8
	Pise12-03B	165-405	55	80	-6	60.6	
	Pise12-03C	170-400	60	78	0	63.3	
Pise12-04	Pise12-04A	155-390	50	80	-3	62.0	61.8±0.5
	Pise12-04B	155-395	55	77	0	61.2	
	Pise12-04D	140-395	55	84	-3	62.2	
Pise12-05	Pise12-05A	150-390	50	71	-3	59.0	60.3±1.4
	Pise12-05B	150-390	55	71	-2	61.8	
	Pise12-05C	140-395	55	81	-2	60.1	
Pise12-06	Pise12-06A	150-390	50	72	1	52.2	52.7±0.5
	Pise12-06E	155-395	55	76	-6	53.2	
Pise12-07	Pise12-07A	150-385	50	81	-3	57.6	58.2±0.5
	Pise12-07B	150-395	55	84	-3	58.5	
	Pise12-07C	150-395	60	86	-2	58.5	
Pise12-09	Pise12-09A	170-385	50	70	-1	59.5	59.5±0.8
	Pise12-09B	145-360	55	62	1	58.7	
	Pise12-09C	140-395	55	79	-1	60.3	
Pise12-10	Pise12-10A	150-385	50	74	-2	59.3	59.5±1.4
	Pise12-10C	150-395	55	77	-1	60.9	
	Pise12-10E	150-395	55	74	4	58.2	
Pise12-11	Pise12-11A	150-400	50	67	-5	57.3	55.9±1.2
	Pise12-11C	140-395	55	71	0	55.0	
	Pise12-11D	140-395	55	71	-2	55.5	
Pise12-12	Pise12-12A	150-390	50	87	-1	52.2	53.1±1.0
	Pise12-12B	150-375	55	89	-2	52.9	
	Pise12-12C	150-390	55	87	-1	54.2	
Pise11, Pisa, Medieval walls, [1300-1350] AD, (14/9/4)*							
Pise11-01	Pise11-01A	150-400	50	75	1	50.7	50.9±0.2
	Pise11-01C	155-390	50	66	-4	50.9	
	Pise11-01D	160-395	50	63	-4	51.1	
Pise11-02	Pise11-02A	135-390	50	77	-5	52.5	53.0±1.0
	Pise11-02B	140-385	50	75	-9	52.4	
	Pise11-02D	135-390	50	74	-4	54.2	
Pise11-06	Pise11-06A	165-390	50	70	-3	48.7	49.6±1.0
	Pise11-06B	135-390	50	75	-1	50.6	
	Pise11-06C	150-390	50	74	-4	49.5	
Pise11-11	Pise11-11A	150-390	50	73	2	51.7	51.4±1.5
	Pise11-11B	150-400	50	83	2	49.8	
	Pise11-11C	155-390	50	74	-6	52.8	
Pise10, Pisa, New citadel - Santa Barbara Tower, 1440 AD, (16/15/15)*							
Pise10-01	Pise10-01A	150-400	50	76	1	51.9	52.7±0.8
	Pise10-01B	150-400	50	78	-4	53.5	
Pise10-02	Pise10-02A	170-400	50	74	-9	50.5	50.1±0.4
	Pise10-02B	170-385	50	76	-2	49.7	
Pise10-03	Pise10-03A	150-400	50	75	2	51.3	51.8±0.5
	Pise10-03B	150-400	50	74	-1	52.3	
Pise10-05	Pise10-05A	150-400	50	77	-4	52.7	53.1±0.4
	Pise10-05B	150-390	50	78	-5	53.5	
Pise10-06	Pise10-06A	165-400	50	76	-6	51.5	51.8±0.3
	Pise10-06B	165-390	50	76	-4	52.0	
Pise10-07	Pise10-07A	180-400	50	68	-2	51.0	51.6±0.6

	Pise10-07B	180-390	50	75	-3	52.2	
Pise10-08	Pise10-08A	175-385	50	75	5	52.2	52.3±0.1
	Pise10-08B	175-390	50	80	4	52.3	
Pise10-09	Pise10-09A	150-390	50	79	5	47.1	47.8±0.7
	Pise10-09B	150-390	50	77	-4	48.5	
Pise10-10	Pise10-10A	165-395	50	83	-6	47.6	48.8±1.2
	Pise10-10B	165-390	50	77	-6	50.0	
Pise10-11	Pise10-11A	155-400	50	80	-1	45.7	46.7±1.0
	Pise10-11B	155-385	50	78	-3	47.7	
Pise10-12	Pise10-12A	180-390	50	72	-5	48.4	49.6±1.2
	Pise10-12B	150-395	50	79	-3	50.7	
Pise10-13	Pise10-13A	150-395	50	73	-9	52.3	52.2±0.1
	Pise10-13B	150-390	50	80	-5	52.1	
Pise10-14	Pise10-14A	150-400	50	78	0	52.8	53.1±0.3
	Pise10-14B	150-390	50	80	0	53.3	
Pise10-15	Pise10-15A	150-395	50	75	-3	52.0	51.4±0.7
	Pise10-15B	150-390	50	75	-2	50.7	
Pise10-16	Pise10-16A	150-395	50	76	-4	50.9	51.1±0.2
	Pise10-16B	150-390	50	75	-1	51.2	
Pise02, Pisa, Oratory of San Bernardino, [1479-1490] AD, (12/12/11)*							
Pise02-01	Pise02-01A	180-400	50	73	0	46.9	48.0±1.1
	Pise02-01B	140-385	50	80	3	49.0	
Pise02-02	Pise02-02A	180-400	50	85	-2	46.2	46.9±0.7
	Pise02-02B	140-395	50	82	-2	47.6	
Pise02-03	Pise02-03C	135-380	50	67	-4	51.9	51.4±0.6
	Pise02-03D	135-385	50	68	1	50.8	
Pise02-04	Pise02-04A	170-420	50	95	1	46.9	47.9±1.0
	Pise02-04B	145-400	50	94	-4	48.9	
Pise02-05	Pise02-05A	165-420	50	85	-3	47.0	47.9±0.9
	Pise02-05B	140-385	50	83	-2	48.8	
Pise02-06	Pise02-06A	160-410	50	91	-1	46.6	47.5±0.9
	Pise02-06B	140-385	50	91	-2	48.4	
Pise02-07	Pise02-07A	165-400	50	78	-2	49.7	49.6±0.2
	Pise02-07B	150-365	50	80	-2	49.4	
Pise02-08	Pise02-08A	150-400	50	57	-5	51.1	51.0±0.1
	Pise02-08B	140-395	50	75	-2	50.9	
Pise02-09	Pise02-09B	140-395	50	82	0	48.8	48.9±0.1
	Pise02-09C	135-385	50	82	0	49.0	
Pise02-10	Pise02-10A	150-400	50	89	-4	45.3	45.8±0.5
	Pise02-10B	145-400	50	89	-3	46.2	
Pise02-11	Pise02-11A	160-400	50	67	-2	48.9	49.9±1.0
	Pise02-11B	155-385	50	70	-5	50.9	
Pise09, Pisa, New Citadel - Sangallo bastion, [1531-1533] AD, (12/5/5)*							
Pise09-02	Pise09-02A	150-400	50	68	-7	50.3	51.1±1.1
	Pise09-02B	170-400	50	68	-6	52.4	
	Pise09-02C	150-405	50	71	2	50.6	
Pise09-04	Pise09-04A	180-465	50	84	2	50.2	51.6±1.3
	Pise09-04B	185-400	50	82	-7	51.9	
	Pise09-04D	175-390	50	80	-7	52.7	
Pise09-08	Pise09-08A	155-410	50	83	-7	52.8	51.9±0.9
	Pise09-08B	150-400	50	83	-1	51.1	
	Pise09-08C	150-405	50	87	-3	51.9	
Pise09-10	Pise09-10A	150-410	50	79	2	50.9	52.5±1.4
	Pise09-10B	150-390	50	79	-2	53.3	
	Pise09-10C	150-405	50	82	0	53.2	
Pise09-12	Pise09-12A	150-410	50	94	-3	49.9	51.5±1.4
	Pise09-12B	150-390	50	76	-4	52.5	
	Pise09-12D	150-395	50	87	-5	52.2	
Pise01, Pisa, "Le Bocchette di Putignano", 1558 AD, (10/3/3)*							
Pise01-07	Pise01-07A	175-400	50	60	0	46.7	47.1±0.4

	Pise01-07B	175-445	50	70	5	47.1	
	Pise01-07C	175-450	50	70	4	47.4	
Pise01-08	Pise01-08A	150-400	50	70	-4	50.7	51.3±1.1
	Pise01-08B	140-395	50	74	-3	52.5	
	Pise01-08C	175-395	50	72	-5	50.6	
Pise01-10	Pise01-10A	150-400	50	72	2	51.8	53.0±1.1
	Pise01-10B	140-395	50	69	4	53.1	
	Pise01-10D	155-395	50	69	-1	54.0	
Pise08, Pisa, Medici shipyard (Arsenal), 1588 AD, (15/11/6)*							
Pise08-03	Pise08-03A	155-400	50	80	-6	54.9	55.1±0.2
	Pise08-03B	160-395	50	78	-1	55.2	
Pise08-04	Pise08-04A	150-400	50	76	2	52.0	52.6±0.6
	Pise08-04B	145-385	50	79	1	53.2	
Pise08-05	Pise08-05A	135-390	50	82	-9	50.6	51.0±0.4
	Pise08-05B	135-390	50	84	-5	51.3	
Pise08-06	Pise08-06A	150-400	50	79	-1	54.9	54.8±0.2
	Pise08-06B	145-385	50	82	6	54.6	
Pise08-08	Pise08-08A	150-395	50	61	-6	51.8	51.4±0.4
	Pise08-08B	150-420	50	70	-7	51.0	
Pise08-11	Pise08-11A	150-390	50	82	1	53.4	53.6±0.2
	Pise08-11B	145-385	50	81	0	53.8	
Pise06, Pisa, Medici Aqueduct - Arch, 1595 AD, (15/15/12)*							
Pise06-01	Pise06-01A	150-400	55	84	-4	54.8	54.6±0.2
	Pise06-01B	150-390	55	81	0	54.4	
Pise06-02	Pise06-02A	165-400	55	83	-1	50.9	52.1±1.2
	Pise06-02B	165-390	50	81	-5	53.3	
Pise06-03	Pise06-03A	150-400	55	80	0	53.7	55.1±1.4
	Pise06-03B	150-390	55	82	-3	56.4	
Pise06-04	Pise06-04A	150-400	55	85	-2	51.9	52.9±1.0
	Pise06-04B	150-390	55	86	-2	53.9	
Pise06-05	Pise06-05A	150-400	55	81	-4	54.7	55.1±0.4
	Pise06-05B	150-390	55	80	-1	55.4	
Pise06-07	Pise06-07A	150-400	55	86	0	54.5	54.6±0.1
	Pise06-07B	150-390	55	85	-1	54.7	
Pise06-08	Pise06-08A	150-400	55	83	0	52.3	53.3±1.0
	Pise06-08B	150-390	55	80	-7	54.2	
Pise06-09	Pise06-09A	150-400	55	84	-1	53.8	55.0±1.2
	Pise06-09B	150-390	55	83	-2	56.1	
Pise06-10	Pise06-10A	150-400	55	80	-3	55.1	55.5±0.4
	Pise06-10B	150-390	55	86	-2	55.9	
Pise06-11	Pise06-11A	150-400	55	79	-4	54.9	55.0±0.1
	Pise06-11B	150-390	55	82	-1	55.1	
Pise06-12	Pise06-12B	150-385	55	88	-3	54.1	53.3±0.8
	Pise06-12D	150-395	55	93	1	52.5	
Pise06-13	Pise06-13A	150-400	55	81	-7	56.2	56.8±0.6
	Pise06-13B	150-390	55	82	-5	57.4	
Pise07, Pisa, Santo Stefano dei Cavalieri church, [1683-1691] AD, (12/12/12)*							
Pise07-01	Pise07-01A	150-400	45	76	2	49.9	50.8±0.9
	Pise07-01B	150-390	50	78	4	51.6	
Pise07-02	Pise07-02A	150-390	45	86	0	50.3	51.4±1.1
	Pise07-02B	150-395	50	82	1	52.5	
Pise07-03	Pise07-03A	145-400	45	74	1	50.2	51.4±1.2
	Pise07-03B	170-395	50	81	2	52.6	
Pise07-04	Pise07-04A	150-400	50	86	3	50.8	50.6±0.3
	Pise07-04B	145-395	50	87	-2	50.3	
Pise07-05	Pise07-05A	150-400	50	85	-2	50.8	51.2±0.4
	Pise07-05B	140-395	50	85	0	51.6	
Pise07-06	Pise07-06A	175-395	50	81	-5	46.8	46.6±0.3
	Pise07-06B	190-395	50	81	0	46.3	
Pise07-07	Pise07-07A	150-400	50	79	-4	50.5	50.5±0.1

	Pise07-07B	145-395	50	80	-2	50.4	
Pise07-08	Pise07-08A	150-400	50	84	0	49.4	50.2±0.8
	Pise07-08B	145-400	50	82	1	51.0	
Pise07-09	Pise07-09A	150-400	50	82	2	51.4	52.2±0.8
	Pise07-09B	140-395	50	82	0	52.9	
Pise07-10	Pise07-10A	150-390	50	89	-1	51.3	51.2±0.2
	Pise07-10B	145-395	50	90	1	51.0	
Pise07-11	Pise07-11A	140-395	50	82	-3	48.2	47.2±1.1
	Pise07-11B	155-385	50	70	1	46.1	
Pise07-12	Pise07-12A	150-395	50	88	4	48.5	49.3±0.8
	Pise07-12B	140-395	50	90	3	50.1	

Pise03, Asciano Pisano, Medici Aqueduct - Cistern, [1613-1617] AD, (12/11/10)*

Pise03-01	Pise03-01A	155-420	50	78	1	54.4	55.0±0.6
	Pise03-01B	150-400	50	78	-4	55.6	
Pise03-02	Pise03-02A	150-400	50	73	4	53.9	55.2±1.3
	Pise03-02B	150-385	50	75	-2	56.4	
Pise03-03	Pise03-03A	150-400	55	80	0	54.2	54.1±0.1
	Pise03-03B	150-385	55	80	1	54.0	
Pise03-05	Pise03-05A	150-400	55	79	-1	56.0	56.5±0.5
	Pise03-05B	150-385	55	74	-2	56.9	
Pise03-06	Pise03-06A	150-400	55	81	0	54.9	55.8±0.9
	Pise03-06C	150-380	55	82	-3	56.6	
Pise03-07	Pise03-07A	150-400	55	81	-1	54.4	55.7±1.3
	Pise03-07B	145-385	55	80	-3	57.0	
Pise03-08	Pise03-08B	135-385	55	80	0	57.5	58.1±0.6
	Pise03-08C	135-380	55	79	2	58.7	
Pise03-09	Pise03-09A	150-400	55	78	-2	52.6	52.4±0.3
	Pise03-09B	150-385	55	78	2	52.1	
Pise03-10	Pise03-10A	150-400	55	87	-5	53.1	52.1±1.1
	Pise03-10B	150-390	55	87	-2	51.0	
Pise03-11	Pise03-11A	150-400	55	72	1	54.7	54.7±0.0
	Pise03-11B	150-390	55	79	2	54.7	

Pise04, Asciano Pisano, Medici Aqueduct - Pillar, [1613-1617] AD, (12/11/9)*

Pise04-01	Pise04-01A	150-400	55	93	-2	51.6	53.0±1.2
	Pise04-01B	140-390	55	89	1	53.7	
	Pise04-01D	140-380	55	93	2	53.8	
Pise04-02	Pise04-02A	150-400	55	81	-3	51.2	52.4±1.2
	Pise04-02B	170-390	55	84	-3	53.6	
Pise04-04	Pise04-04A	150-400	55	81	1	54.2	55.5±1.3
	Pise04-04B	140-390	55	87	1	56.8	
	Pise04-04C	140-395	55	84	-1	55.6	
Pise04-05	Pise04-05A	150-400	55	85	0	56.3	56.9±1.0
	Pise04-05B	140-390	55	82	-3	56.4	
	Pise04-05D	150-385	55	88	0	58.1	
Pise04-06	Pise04-06A	170-390	55	80	-5	49.8	50.5±0.7
	Pise04-06B	150-395	55	83	-3	51.1	
Pise04-07	Pise04-07A	160-400	55	82	-4	56.5	56.8±0.2
	Pise04-07B	165-390	55	79	-5	56.9	
	Pise04-07C	165-395	55	82	-4	56.9	
Pise04-10	Pise04-10A	150-400	55	79	2	55.9	56.5±0.6
	Pise04-10B	150-390	55	84	-1	57.1	
Pise04-11	Pise04-11A	150-400	55	80	0	54.8	55.7±0.9
	Pise04-11B	150-390	55	86	-2	56.5	
Pise04-12	Pise04-12A	150-400	55	88	-5	55.8	56.6±0.8
	Pise04-12B	150-390	55	88	-3	57.4	

Pise05, Asciano Pisano, Medici Aqueduct - Pillar, 1632 AD, (14/13/13)*

Pise05-01	Pise05-01A	150-400	50	76	-1	53.0	52.9±0.1
	Pise05-01B	150-370	50	77	-2	52.8	
Pise05-02	Pise05-02A	150-400	50	87	2	50.5	51.0±0.5
	Pise05-02B	150-400	50	83	1	51.5	

Pise05-03	Pise05-03A	150-400	50	79	-4	52.8	53.4±0.6
	Pise05-03B	150-380	50	75	-6	53.9	
Pise05-04	Pise05-04A	150-400	50	81	-4	55.3	54.3±1.1
	Pise05-04B	150-380	50	82	-4	53.2	
Pise05-05	Pise05-05A	150-400	50	89	2	51.1	52.0±0.9
	Pise05-05B	150-385	50	89	-1	52.9	
Pise05-06	Pise05-06A	150-400	50	80	0	51.2	52.1±0.8
	Pise05-06B	150-385	50	80	1	52.9	
Pise05-07	Pise05-07A	150-400	50	83	0	54.3	55.0±0.7
	Pise05-07B	150-390	50	82	-2	55.6	
Pise05-09	Pise05-09A	150-400	50	84	3	54.9	55.5±0.6
	Pise05-09B	150-390	50	84	0	56.1	
Pise05-10	Pise05-10B	140-385	50	88	-3	53.4	53.3±01
	Pise05-10C	140-385	50	84	-3	53.2	
Pise05-11	Pise05-11A	150-400	50	81	-1	54.6	54.9±0.3
	Pise05-11B	160-390	50	79	-2	55.1	
Pise05-12	Pise05-12A	175-375	50	68	4	51.2	50.6±0.7
	Pise05-12B	170-390	50	75	-7	49.9	
Pise05-13	Pise05-13A	135-380	50	72	-6	50.9	52.1±1.2
	Pise05-13C	140-380	50	73	1	53.3	
Pise05-14	Pise05-14A	150-395	50	79	4	52.4	53.7±1.3
	Pise05-14B	150-385	50	80	-1	55.0	

Tosc03, Calcinaia, Castle - Medieval Tower, [1260-1287] AD, (11/10/5)*

Tosc03-05	Tosc03-05A	190-445	50	78	5	50.7	50.1±0.7
	Tosc03-05B	190-435	50	79	-6	49.4	
Tosc03-06	Tosc03-06A	140-445	50	81	7	50.6	49.6±1.1
	Tosc03-06B	135-425	50	82	3	48.5	
Tosc03-07	Tosc03-07A	220-445	50	70	3	52.0	52.4±0.4
	Tosc03-07B	220-435	50	75	0	52.7	
Tosc03-08	Tosc03-08A	140-445	50	75	4	55.1	56.0±0.9
	Tosc03-08B	160-435	50	72	5	56.8	
Tosc03-10	Tosc03-10A	140-445	50	84	-3	53.3	53.3±0.0
	Tosc03-10B	150-435	50	75	-3	53.2	

Tosc04, Marti, Santa Maria Novella church, 1331 AD, (12/11/10)*

Tosc04-02	Tosc04-02A	170-400	55	71	-4	49.0	48.3±0.7
	Tosc04-02B	155-380	55	66	-7	47.6	
	Tosc04-02E	155-395	55	70	-2	48.3	
Tosc04-03	Tosc04-03A	155-400	55	85	-3	46.1	47.1±1.0
	Tosc04-03B	135-380	55	86	-2	48.1	
Tosc04-05	Tosc04-05A	140-395	55	86	2	55.1	55.9±0.8
	Tosc04-05B	140-390	45	86	-4	56.6	
Tosc04-06	Tosc04-06A	140-395	55	85	4	52.1	53.0±0.9
	Tosc04-06B	140-390	55	81	-5	53.9	
Tosc04-07	Tosc04-07A	140-395	55	89	-2	55.1	55.3±0.2
	Tosc04-07B	140-390	55	89	-5	55.4	
Tosc04-08	Tosc04-08A	140-395	55	82	-1	54.1	54.3±0.2
	Tosc04-08B	135-380	55	81	1	54.5	
Tosc04-09	Tosc04-09A	140-395	55	81	2	48.1	48.8±0.7
	Tosc04-09B	135-380	55	82	-1	49.5	
Tosc04-10	Tosc04-10A	140-395	55	85	2	53.5	54.6±1.1
	Tosc04-10B	145-380	55	83	-4	55.7	
Tosc04-11	Tosc04-11A	140-395	55	83	4	54.8	55.1±0.3
	Tosc04-11B	140-380	55	85	2	55.3	
Tosc04-12	Tosc04-12A	140-395	55	79	4	50.3	51.4±1.1
	Tosc04-12B	140-390	55	77	-1	52.4	